NTNU

Norwegian University of
Science and Technology

Experimental Study of Hydraulic Accumulator Discharge

Marcus Aleksander Stenhjem

Subsea Technology
Submission date: June 2018
Supervisor: Olav Egeland, MTP
Co-supervisor: Boris Balakin, HVL
Gleb Pisarev, OneSubsea

Norwegian University of Science and Technology
Department of Mechanical and Industrial Engineering

Abstract

This thesis aims to identify the behaviour of a 4 l hydraulic bladder accumulator undergoing discharge under various conditions and ultimately shed some light on irregularities that OneSubsea Processing is experiencing regarding rapid initial pressure reduction in one of their off-shore accumulator systems connected to a subsea multiphase pump with a hydraulic umbilical.

An analytical solution for P(t) in the accumulator has been developed and has shown high levels of accuracy provided that the discharge coefficient of the orifice that the accumulator discharges through is calculated properly. The means of identifying and using the discharge coefficient has been thoroughly documented.

The impact of changing the working conditions for the accumulator such as altering glycol concentrations in the hydraulic fluid, varying its surrounding temperature, changing pre-charge pressure in the accumulator and changing the valve orifice of which the accumulator discharges through have all been researched. The change of glycol concentration in the hydraulic fluid also alters viscosity. The fluid viscosity increases exponentially with the glycol concentration, which is also the case regarding the time it takes to discharge the accumulator. Altering the temperature of the accumulator impacts fluid viscosity as well. However, the most substantial impact of temperature alteration has proven to be the change in internal energy of the gas in the accumulator and how it affects the final charge pressure.

Tests where an accumulator is installed at an elevation and connected to a long tube in effort to replicate an umbilical system has given insight into how the discharge is affected by gravitational and frictional force. Multiple tests at different elevations and tube lengths have shown how the tube friction and gravitational force work against each other when discharge commences. In this specific study, a tube height to length travelled ratio of 1:1.9 resulted in the two forces cancelling each other out.

An isothermal experiment where the accumulator was discharged at a rate of 1.08 l/h shows similar results to those documented by OneSubsea regarding pressure reduction, and indicates thermal losses in the gas as being partly the cause of the accelerated pressure reduction in the start of the discharge cycle.

Sammendrag

Denne oppgaven har som mål å kartlegge oppførselen til en 4 l hydraulisk blæreakkumulator som gjennomgår discharge under ulike arbeidsforhold og til slutt belyse uregelmessigheter som OneSubsea Processing opplever når det gjelder rask innledende trykkreduksjon i et av deres off-shore akkumulatorsystemer koblet til en subsea flerfasepumpe ved bruk av en hydraulisk umbilical.

En analytisk løsning for P(t) i akkumulatoren er utviklet og har vist høy grad av nøyaktighet forutsatt at discharge-koeffisienten for åpningen som akkumulatoren discharger gjennom er beregnet riktig. Metoden brukt for å identifisere og bruke discharge-koeffisienten er grundig dokumentert.

Virkningen av å variere arbeidsforholdene i form av å endre glykolkonsentrasjoner i hydraulikkvæsken, variere omgivende temperatur, endre pre-charge i akkumulatoren og å justere ventilåpningen som akkumulatoren discharger gjennom har alle blitt undersøkt. Forandringen av glykolkonsentrasjon i hydraulikkvæsken endrer også viskositeten. Væskeviskositeten øker eksponentielt med glykolkonsentrasjonen, som også er tilfellet hva angår tiden det tar å discharge akkumulatoren. Å endre temperaturen på akkumulatoren påvirker også væskeviskositeten. Imidlertid har den mest omfattende effekten av temperaturendring vist seg å være endringen i gassens indre energi i akkumulatoren, og hvordan det påvirker det initielle trykket i akkumulatoren før discharge.

Tester hvor en akkumulator er installert på en gitt høyde og koblet til en lang slange i et forsøk på å gjenskape et umbilical-system har gitt innsikt i hvordan discharge påvirkes av tyngdekraft og friksjonskraft. Flere tester i forskjellige høyder og slangelengder har vist hvordan rørfriksjonen og gravitasjonskraften virker mot hverandre når discharge initieres. I denne spesifikke studien resulterte et rørhøyde til lengde-forhold på 1:1.9 i at de to kreftene jevnet hverandre ut.

Et isotermisk eksperiment hvor akkumulatoren ble discharget med en hastighet på 1.08 l/h viser lignende resultater som de som ble dokumentert av OneSubsea angående trykkreduksjon, og indikerer termiske tap i gassen som delvis årsaken til den akselererte trykkreduksjonen i starten av discharge-syklusen.

Preface

This Master thesis is submitted in partial fulfilment of the requirements for obtaining a Master of science degree in Subsea Technology, Operations and Maintenance at the Norwegian University of Science and Technology (NTNU) in collaboration with OneSubsea Processing AS, and presents the results of a 5-month long project which begun the 15th of January 2018 until the 11th of June 2018.

I would like to express my gratitude to my academic supervisor Boris V. Balakin for his help and support with discussing the project and giving feedback throughout its entirety. Also, i would like to thank the Department of Mechanical and Marine Engineering at the Western Norway University of Applied Sciences for supplying the project with the necessary facilities and equipment. I would also like to thank Gleb Pisarev at OneSubsea Processing AS for giving me the opportunity to take part in this project. I would also like to express my gratitude to Espen Hiis and Jorge Gómez Vidal for helping me conduct some of the more demanding experiments when needed. Finally, I would like to thank HyCom AS for their generous donation of a hydraulic bladder accumulator for this project.

Bergen, 11. June 2018

Marcus A. Stenhjem

Contents

List of Tables

List of Figures

Abbreviations

$\hat{\mu}$	=	Discharge coefficient
μ	=	Dynamic viscosity
ν	=	Kinematic viscosity
τ_s	=	Shear rate
τ	=	Thermal time constant
τ_t	=	Transmissivity
m	=	Mass
U	=	Internal energy
W	=	Work
Q_v	=	Volume flow
Q_h	=	Amount of heat
q	=	Heat flux
V	=	Volume
c_p	=	Specific heat of gas at constant pressure
c_v	=	Specific heat of gas at constant volume
R	=	Gas constant
T	=	Temperature
T_a	=	Temperature
p	=	Pressure
A	=	Area
α	=	Thermal diffusivity
α_a	=	Absorptivity
k	=	Thermal conductivity of material
t	=	Time
ρ	=	Density
ρ_r	=	Reflectivity
ϵ	=	Emissivity
W	=	Radiation power
σ	=	Steffan-Botzltzmann constant
σ_s	=	True standard deviation
h	=	Heat transfer coefficient
v	=	Velocity
g	=	Gravitational acceleration
z	=	Elevation
D	=	Diameter
Ω	=	Electrical resistance (Ohm)
γ	=	Heat capacity ratio of a gas
ϕ	=	Angle
C	=	Constant

Chapter 1

Introduction

In the summer of 2017, i was contacted by OneSubsea, a Schlumberger company, and a potential research assignment was presented. OneSubsea said that they were having problems with unforeseen pressure reduction in their off-shore hydraulic accumulators. In the spring of 2017, a bachelor project was written for OneSubsea where two students simulated a fluid-barrier system containing hydraulic accumulators, using fluidsim (Haugland and Wikan, 2017). The results from this assignment showed promise with respect to how well the simulations corresponded with OneSubsea's field data. Field data from one of OneSubsea's off-shore accumulators can be seen in figure 1.1, where the rapid pressure reduction at the start of operation is easily identified in six separate periods of discharge. The working theory at this point was that there could be a leak in the hydraulic umbilical which was going from the accumulator to a subsea multiphase pump.

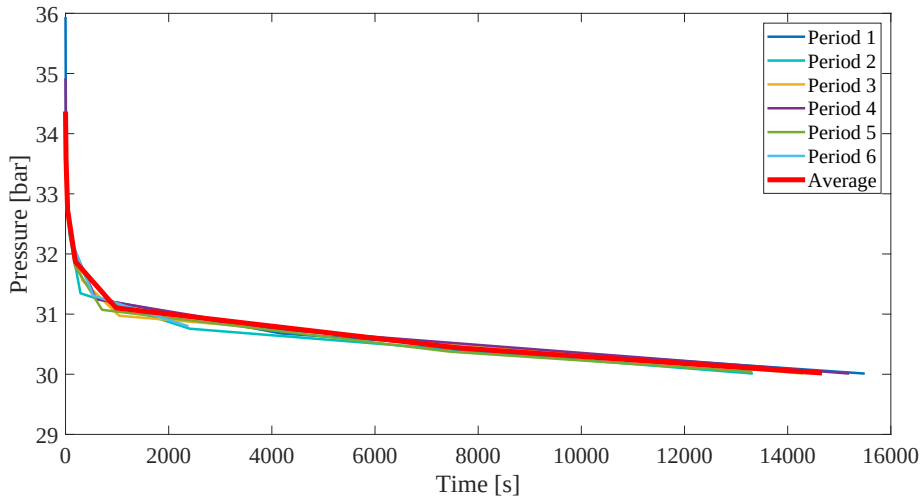

Figure 1.1: Graph of the accumulator field data provided by OneSubsea from an off-shore installation.

The scope of this master's thesis is to analyse a hydraulic accumulator and its behaviour upon discharge at various conditions. Parallel to this work, a CFD-model is created by a fellow student, where some of the experimental results from this thesis will be recreated. To make these tests possible, an experimental setup is needed. The work with making such a setup started in the fall of 2017 and continued a few weeks into the spring of 2018.

1.1 Thesis Objective

This master's thesis is made in collaboration with OneSubsea, a Schlumberger company, that delivers integrated solutions, products systems and services for increased reservoir recovery for the subsea oil and gas market. OneSubsea is interested in having a closer look at hydraulic accumulators regarding their behaviour upon discharge when used for leak compensation. The project is divided into two separate sub-projects, where one will focus on experimental work on an accumulator, while the other will develop a CFD-model that can be validated against the experimental data. The end goal is to present OneSubsea with a realistic CFD-model that eventually can be used when designing systems where hydraulic accumulators are involved.

1.2 Literature Review

The hydraulic accumulator is a type of high pressure container used to store or supply energy from pressure. Today the most used forms of accumulators are gas charged, or closed accumulators. A hydraulic accumulator can serve several purposes in a hydraulic system. It can act as a supplier of pressure in a system that is lacking a pump, or where a pump is temporarily removed. It can serve as an extra supply of pressure in systems where the pumps are too small to deliver the maximum load required by the system. An accumulator can maintain a steady pressure in systems experiencing leaks or volume changes due to fluctuations in temperature. Accumulators can also compensate for pressure pulsations in a system due to uneven supply from pumps and absorb shocks due to for example suddenly closing a valve (Kjølle, 1989).

Active charge accumulator, or ACA, is an example of accumulators used to compensate for sudden shocks of pressure in a system. Yoshida et al. (2017) has conducted experimental work on an ACA used to regulate pressure in a system that uses different hydraulic pressure levels for various tasks. This enables a system to use one pressure source and later convert it to multiple levels of pressure by adding separate sections controlled by pressure transducer steered valves for pressure reduction. The study resulted in an analytical solution for the pressure reduction in the system that was verified by experiments and showed how increased load flow rate also increased the number of charge/discharge cycles in the system.

Rydberg (2015) considers the hydraulic accumulator and hydraulic fluid as the most important component in an energy efficient hydraulic system. He identifies the importance of considering the characteristics of them both. Rydberg mentions thermal losses as the dominant cause of flow loss in the hydraulic accumulator and shows that these losses are

highly dependent on the frequency of fluid volume change in the accumulator. Rydberg has also earlier identified hydraulic fluids as one of the most important components in a hydraulic system (Rydberg, 2013). The reason for this is that it handles the whole systems energy transfer as well as providing lubrication and cooling. Rydberg has used experimental data (Singireddy and Javalagi, 2012) to successfully validate theoretical calculations for viscosity dependent losses in hydraulic pipes and is able to conclude that the efficiency of a hydraulic system is highly dependent upon the viscosity of the hydraulic fluid being used.

Pourmovahed and Otis (1990) has further investigated their earlier work (Otis and Pourmovahed, 1985) regarding the thermal time constant by means of experiments which have been used for validation. This work resulted in a renewed equation for determining the thermal time coefficient for both horizontal and vertical orientation of an accumulator.

Juhala et al. (2014) identified a lack of literature where piston, bladder and diaphragm accumulators all are compared from an energy efficiency point of view. Therefore, experimental tests were carried out for piston, bladder and diaphragm accumulators. The work done by Pourmovahed and Otis (1990) is used to establish the thermal time constant and the corresponding experimental results show a higher degree of energy efficiency in both the bladder and diaphragm accumulator compared to the piston accumulator due to the bladder material and its isolating properties.

1.3 Thesis outline

This thesis is divided into 7 chapters, where the first chapter is meant to give a brief introduction to the project and why it is of interest. The following three chapters describes the theory used in the thesis, how the experimental setup was built, and materials gathered to be able to properly test a hydraulic accumulator. The next two chapters describes in detail all the experiments that are carried out and the results from them. The last chapter concludes on the results and findings of interest in the thesis.

- Chapter 2 describes the underlying theory in the thesis with respect to the thermodynamics and heat transfer behaviour of a hydraulic accumulator, thermal time constant calculation and fluid dynamics.
- Chapter 3 describes the experimental setup used in the thesis. All components are documented, and their objectives and functions are explained.
- Chapter 4 gives an overlook of parameters and calculations that needed to be identified in advance of the main experiments. The parameters and calculation in question is fluid properties, discharge coefficients, thermal time constants and validation of an analytical solution that has been derived.
- Chapter 5 describes all the planned experiments in detail with respect to pre-charge pressure, temperatures, valve orifice, fluid properties and accumulator placement and elevation.
- Chapter 6 presents and discusses all the experimental results that have been obtained.

- Chapter 7 rounds up the thesis with concluding remarks with respect to the results and mentions important findings made before giving recommendations for future related work.

Chapter 2

Theory

2.1 Thermodynamics of hydraulic accumulators

The behaviour of the gas that a hydraulic accumulator is pre-charged with has great influence on the behaviour of the accumulator. Three states can be described for an accumulator when explaining the thermodynamics of the gas (Kjølle, 1989).

- p_0, V_0 and T_0 = The pressure, volume and temperature of the pre-charged gas in the accumulator
- p_1, V_1 and T_1 = The pressure, volume and temperature of the gas when the accumulator is fully charged with hydraulic oil
- p_2, V_2 and T_2 = The pressure, volume and temperature of the gas when the accumulator reaches its minimum operational pressure

The mass of the gas is determined by using the equation of state

$$m = \frac{p_0 V_0}{R T_0} \tag{2.1}$$

where R is the gas constant, described as the difference between the specific heat of the gas at constant pressure (c_p) and the specific heat of the gas at constant volume (c_v). The internal energy of the gas is given by

$$U_1 = m c_v T \tag{2.2}$$

When an accumulator is undergoing charging, the gas is being compressed and work (ΔW_1) defined as negative is being performed on the gas. Further the gas emits heat (ΔQ), which is also defined as negative. Following the first law of thermodynamics, we get

$$\Delta U_1 = \Delta W_1 - \Delta Q_1 \tag{2.3}$$

While discharging the accumulator, the gas now expands and pushes fluid out of the accumulator. The work performed on the gas is now positive, and so is the heat emitted, expressed as

$$\Delta U_1 = \Delta Q_1 - \Delta W_1 \tag{2.4}$$

Isothermal process

An isothermal process is defined as a process where no energy from heat is stored in the gas but is transferred to its surroundings entirely, or in other words;

$$T_0 = T_1 = T_2 \tag{2.5}$$

$$\Delta U_1 = \Delta U_2 = 0 \tag{2.6}$$

Further, Equation 2.3 and 2.4 can be re-written as

$$\Delta W_1 = \Delta Q_1 = p_0 V_0 ln \frac{p_1}{p_0} \tag{2.7}$$

and

$$\Delta W_2 = \Delta Q_2 = p_0 V_0 ln \frac{p_1}{p_2} \tag{2.8}$$

Adiabatic process

In the case where the gas in the accumulator undergoes adiabatic process, there is no heat transfer between the gas and its environment, meaning that all energy added to the gas is assumed to be the total change in energy of the gas meaning that

$$\Delta Q_1 = \Delta Q_2 = 0 \tag{2.9}$$

giving

$$\Delta W_1 = \Delta U_1 = m c_v (T_1 - T_0) \tag{2.10}$$

$$\Delta W_2 = -\Delta U_2 = -m c_v (T_2 - T_1) = m c_v (T_1 - T_2) \tag{2.11}$$

In reality the change of state in the gas will be a mix of the isothermal and adiabatic process, meaning that some energy is stored in the gas as an increase in internal energy, while some energy is exchanged with the accumulator's surroundings.

Isochoric process

Another phenomenon that needs consideration when discussing the thermodynamic behaviour of the hydraulic accumulator is the isochoric process, also known as the *constant volume process*. The isochoric process occurs when an accumulator is charged with fluid and the temperature in the gas has increased due to compression until the heat accumulated in the gas equalizes with its surroundings. The heat transferred from the gas, through the accumulator shell and on to its surroundings results in a decrease in internal energy in the gas, which in this case means reduced pressure without changing the volume of the gas. To establish the isochoric process, it is important that the accumulator does not discharge any fluid, as this would allow a change in volume. The equation for work can be described as

$$\Delta W = P \Delta V \tag{2.12}$$

going back to the first equation of thermodynamics, we know that

$$\Delta U = \Delta Q - \Delta W \tag{2.13}$$

In the case of an isochoric process, ΔV = 0, giving

$$\Delta U = \Delta Q \tag{2.14}$$

The expected reduction in pressure due to lower temperatures, can be estimated by using *Gay-Lussac's pressure and temperature law*, which states that the pressure of a given amount of gas held at constant volume is directly proportional to the kelvin temperature.

$$\frac{p}{T} = C \tag{2.15}$$

2.2 Heat transfer analysis of hydraulic accumulators

A hydraulic accumulator may exchange heat with its surroundings during operation. Both convective and conductive heat transfer occurs from the gas to the accumulator shell. This is also the case for the hydraulic fluid that is in direct contact with the accumulator shell. The accumulator shell will also experience conduction and will ultimately radiate and convect heat to its environment. All the three thermal phenomena mentioned are described further in the following sections.

Thermal conductivity

Thermal conductivity is heat transfer in the down-gradient direction of temperature due to molecular motion. In simpler terms, heat transfer through direct contact. Conductivity can happen in all types of matter (i.e. liquids, gases and solids), meaning it happens in all the situations described above. When discussing thermal conduction, it is natural to mention Fourier's law

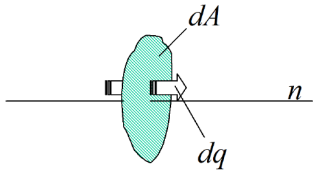

$$\frac{dq}{dA} = -k\frac{\partial T}{\partial n} \tag{2.16}$$

Figure 2.1: Fourier's law (Hoffmann, 2017b)

where $\frac{dq}{dA}$ is the heat flux and k is the conductivity of the material. In the case of a real hydraulic accumulator, the conduction is unsteady, meaning that the temperature varies with time. The heat balance over the element shown in Figure 2.2, can be described as follows

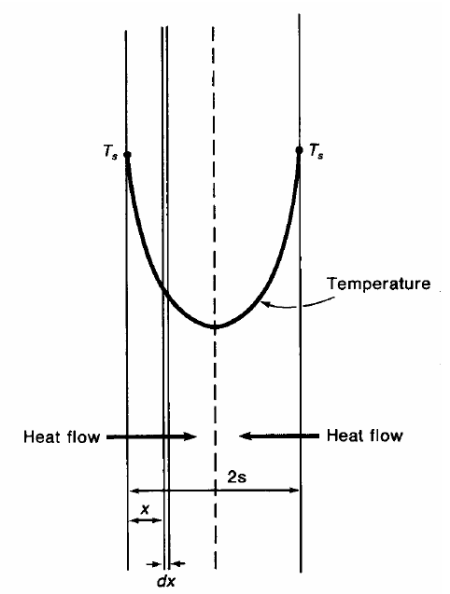

Figure 2.2: Unsteady conduction (Hoffmann, 2017b)

Heat flow in:

$$-kA\frac{\partial T}{\partial x} \tag{2.17}$$

Heat flow out:

$$-kA\Big(\frac{\partial T}{\partial x}+\frac{\partial}{\partial x}\Big(\frac{\partial T}{\partial x}\Big)dx\Big) \tag{2.18}$$

Rate of accumulation:

$$(\rho A dx)C_p\Big(\frac{\partial T}{\partial t}\Big) \tag{2.19}$$

The total balance can be written as the rate of heat accumulation = heat flow in - heat flow out. When simplified, this gives Equation 2.20

$$\frac{\partial T}{\partial t}=\frac{k}{\rho c_p}\frac{\partial^2 T}{\partial x^2}\equiv\alpha\frac{\partial^2 T}{\partial x^2} \tag{2.20}$$

Where α is the thermal diffusivity, k is the thermal conductivity of the material in question, ρ is its density and c_p is the specific heat capacity of the material at constant pressure. The temperature of the domain in a given point can be described with the initial temperature as an example

$$T(x,t=0)=T_0 \tag{2.21}$$

which i turn describes the heat flux at position x = 0

$$-kA\frac{\partial T}{\partial x}[x=0,t]=q_{in} \tag{2.22}$$

Thermal convection

Convection means heat transfer by the flow of fluids, which transports heat with it. There are two types of convection; forced and natural. Forced convection indicates that a flow is initiated through force, while the flow in natural convection is caused by temperature gradients.

Thermal radiation

Thermal radiation is generated through thermal motion in particles in matter. This is true for all matter with a temperature above absolute zero. Total incoming radiation can be divided into three parts; reflectivity (ρ_r), absorptivity (α_a) and transmissivity (τ_t).

To understand radiation, it is important to first understand the definition of a black body. A black body refers to an object with 100 % absorptivity, meaning that no radiation is reflected or pass through the object. Total incoming radiation is explained by Equation 2.23.

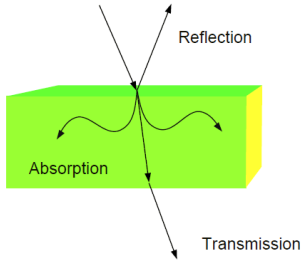

Figure 2.3: Radiation explained (Hoffmann, 2017c)

$$\alpha_a+\rho_r+\tau_t=1 \tag{2.23}$$

whereas a black body would have the given values; α_a = 1, ρ_r = 0 and τ_t = 0 Radiation power, denoted W [$\frac{W}{m^2}$], is the total radiation energy 1 mm^2 of a body emits per second. From this it is possible to describe emissivity (ϵ), which describes a body's radiation power divided by the radiation power of a black body at the same temperature

$$\epsilon=\frac{W}{W_b} \tag{2.24}$$

The Steffan-Boltzmann constant (σ) is a constant that relates the kinetic energy and the temperature of gas particles. To calculate the emitted radiation from a body, the Steffan-Boltzmann constant is required as can be seen in Equation 2.25

$$\frac{q}{A}=\sigma\epsilon T^4 \tag{2.25}$$

$$\sigma(\epsilon_1 T_1^4-\epsilon_2 T_2^4) \tag{2.26}$$

A body will, however, also receive radiation from other bodies in its surrounding. Equation 2.26 describes bodies exchanging radiation where body 1 emits $\sigma\epsilon_1 T_1^4$ while receiving $\sigma\epsilon_2 T_2^4$ from body 2.

2.3 Thermal time constant

Thermal time constants are used when a system is either cooling down or heating up uniformly due to convective cooling or heating and is denoted by the Greek letter τ. The temperature difference between the system and its surroundings is, in this case, proportional to the heat transfer between the system and its surroundings, giving Equation 2.27

$$F = hA_s(T(t) - T_a) \tag{2.27}$$

Where h is the heat transfer coefficient, A_s is the hydraulic fluids surface area inside the accumulator, *T(t)* is the systems temperature at a given time *t* and T_a is the temperature of the systems surroundings.

If the heat from the system is lost to its surroundings, the heat transfer leads to temperature drop in the system, given by Equation 2.28,

$$\rho c_p V \frac{dT}{dt} = -F \tag{2.28}$$

where ρ is the density of the hydraulic fluid, c_p is the specific heat of the fluid and V is the total volume of fluid in the accumulator. The negative sign indicates a reduction in the bodies temperature, giving

$$\rho c_p V \frac{dT}{dt} = -hA_s(T(t) - T_a) \tag{2.29}$$

This can be written in the form given in Equation 2.30

$$\frac{dT}{dt} + \frac{1}{\tau}T = \frac{1}{\tau}T_a \tag{2.30}$$

where τ equals

$$\tau = \frac{\rho c_p V}{hA_s} \tag{2.31}$$

Substituting $(T - T_a)$ with ΔT gives

$$\frac{d\Delta T}{dt} + \frac{1}{\tau}\Delta T = 0 \tag{2.32}$$

Equation 2.32 states that the loss of heat in the system is directly proportional to the temperature difference between the system and it's environment, satisfying Newton's law of cooling. This suggests that ΔT is a function of t, and can be written as shown in Equation 2.33 (Lewis et al., 2004).

$$\Delta T(t) = \Delta T_0 e^{-\frac{t}{\tau}} \tag{2.33}$$

where ΔT_0 is the initial temperature difference between the system and its surroundings.

2.4 Fluid Dynamics

The Bernoulli Equation

A stream line is described as a line going through a flowing fluid in such a way that the velocity vector in any given point is tangent to the line. A stream tube is a tube made up of such stream lines. Kjølle (1989) describes the stream line as shown in Figure 2.4, where v is the flow velocity and A is the cross sectional area of the tube.

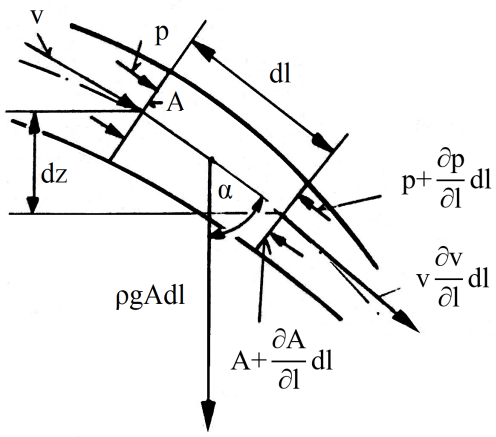

Figure 2.4: Stream tube (Kjølle, 1989)

An element of length dl is defined in the stream tube. The equilibrium state for this element can be described as

$$-A\frac{\partial p}{\partial l}dl - \rho g A dl cos\alpha = \rho A dl \frac{dv}{dt} \tag{2.34}$$

Simplified, we get

$$\frac{1}{\rho}\frac{dp}{dl} + g\frac{dz}{dl} + \frac{dv}{dt} = 0 \tag{2.35}$$

Also

$$\frac{dv}{dt} = \frac{\partial v}{\partial t} + v\frac{\partial v}{\partial l} \tag{2.36}$$

In the case of stationary flow, $\frac{\partial v}{\partial l}$=0. By integrating Equation 2.35, we get

$$p + \rho g z + \frac{\rho v^2}{2} = C \tag{2.37}$$

which is the Bernoulli equation for inviscid, incompressible fluid undergoing stationary flow. On the other hand, if the fluid is considered viscous but still incompressible, the change in energy from one point in the flow to the other is described as

$$p_1 + \rho g z_1 + \frac{\rho v_1^2}{2} = p_2 + \rho g z_2 + \frac{\rho v_2^2}{2} + \Delta p_{loss} \tag{2.38}$$

where Δp_{loss} is the sum of all losses in flow that transforms to heat in the fluid.

Flow through a nozzle

Fluid flowing through a tube with a sudden narrowing of its orifice experiences a significant increase in velocity assuming $A_2 << A_1$, where A_2 is the cross-sectional area of the narrowed orifice, and A_1 is the cross sectional area of the tube. Meaning that $v_1 << v_2$. This enable a simplification of the Bernoulli equation.

$$p_1 = p_2 + \frac{1}{2}\rho v_2^2 \tag{2.39}$$

The velocity through the orifice becomes

$$v_2 = \sqrt{\frac{2\Delta p}{\rho}} \tag{2.40}$$

where Δp = p_1-p_2. The volume flow through the orifice can now be described as

$$Q = v_2 A_2 = A_2\sqrt{\frac{2\Delta p}{\rho}} \tag{2.41}$$

To achieve an analytical solution that corresponds with real experimental results the discharge coefficient, $\hat{\mu}$, which is found empirically is added.

$$Q = A_2\hat{\mu}\sqrt{\frac{2\Delta p}{\rho}} \tag{2.42}$$

Viscosity and shear stress

When a real fluid flows along a stationary wall, the fluid closest to the wall will experience a reduction in its velocity, while fluid in layers further away from the wall will experience an increase in velocity the further from the wall it travels. In other words; we have a velocity gradient $\frac{du}{dy}$ perpendicular to the flow. The shear stress that is being applied to the flow is a result of both the velocity gradient and the fluid viscosity. The relationship between the inertial force and the shear stress creates the dimensionless *Reynolds number* which, for flow in a tube, is expressed as

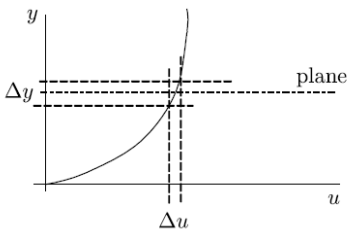

Figure 2.5: Velocity gradient for a fluid close to a stationary wall (Hoffmann, 2017a)

$$R_e = \frac{vD\rho}{\mu} \tag{2.43}$$

where v = mean velocity, D = pipe diameter, ρ is the fluid density and μ = dynamic viscosity. Depending on the magnitude of R_e, one of two flow characteristics will occur; laminar or turbulent flow. The flow

in pipe is considered laminar for $R_e \leq 2300$. This type of flow is considered streamlined. The shear stress per unit area for an arbitrary point for a laminar flow can be expressed as

$$\tau_{yx} = -\mu \frac{du}{dy} \tag{2.44}$$

where τ_{yx} = the stress acting on a y surface in the x-direction and μ = dynamic viscosity. If the Reynolds number exceeds $R_{e_{crit}}$, which is greater than 2300, turbulent flow will occur. The fluid particles will now stop flowing in a streamlined manner, and instead move unpredictably in the flowing direction. The relation between the shear stress and the velocity gradient, will in this case take on a more complex nature without any exact definition. It turns out, however, that it is advantageous to define the shear stress as

$$\tau_{yx} = f\rho \frac{v^2}{2} \tag{2.45}$$

where f is the friction factor. For a pipe, the friction factor is a function of the Reynolds number, the relative roughness of the pipe and the distance from the opening of the pipe.

Chapter 3

Experimental setup

3.1 Configuration

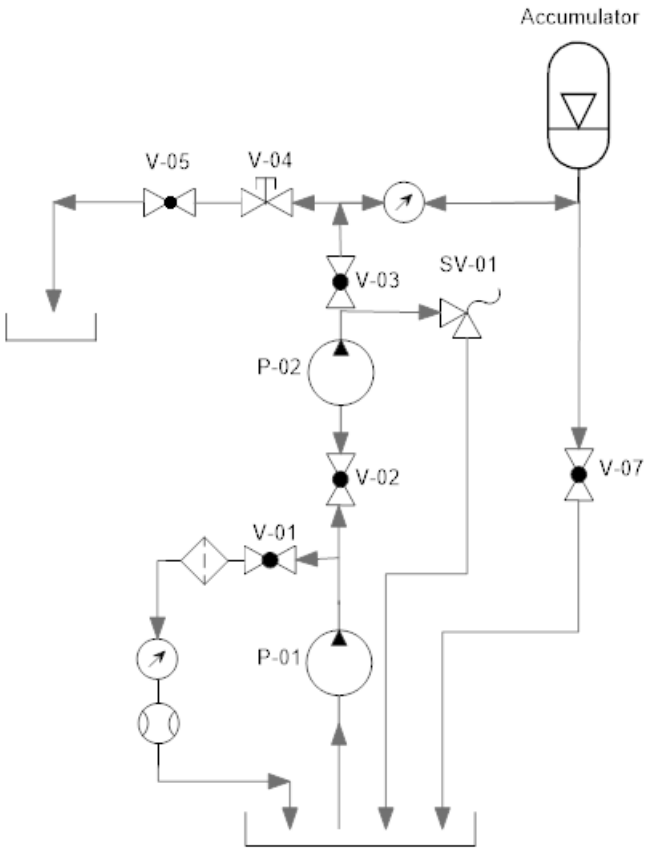

Figure 3.1: PI&D chart of the experimental setup

To charge the accumulator with hydraulic fluid, two centrifugal pumps are installed in series, resulting in a total pressure of 8.8 bars and a maximum flowrate of 55 l/min in the system. The pumps are produced by KÄRCHER, and are called *BP 3 home garden pump*. Between the two pumps, a filtration line is installed. A manometer and a simple water counter is also installed on the filtration line for future educational purposes. A 9-bar safety valve is installed after the second pump.

When filling the accumulator with fluid, firstly, all the air in the tubes must be removed. Valve V-07 is installed for exactly this purpose. When activating the pumps, V-03, V-05 and V-07 are all open. When water is flowing out of both V-05 and V-07, valve V-07 is closed before closing valve V-05. Now the accumulator will start filling with fluid. When the pressure read from manometer before the accumulator shows a pressure of approximately 8.8 bars, valve V-03 is closed before the pumps are turned off. The system is now pressurized and ready for testing.

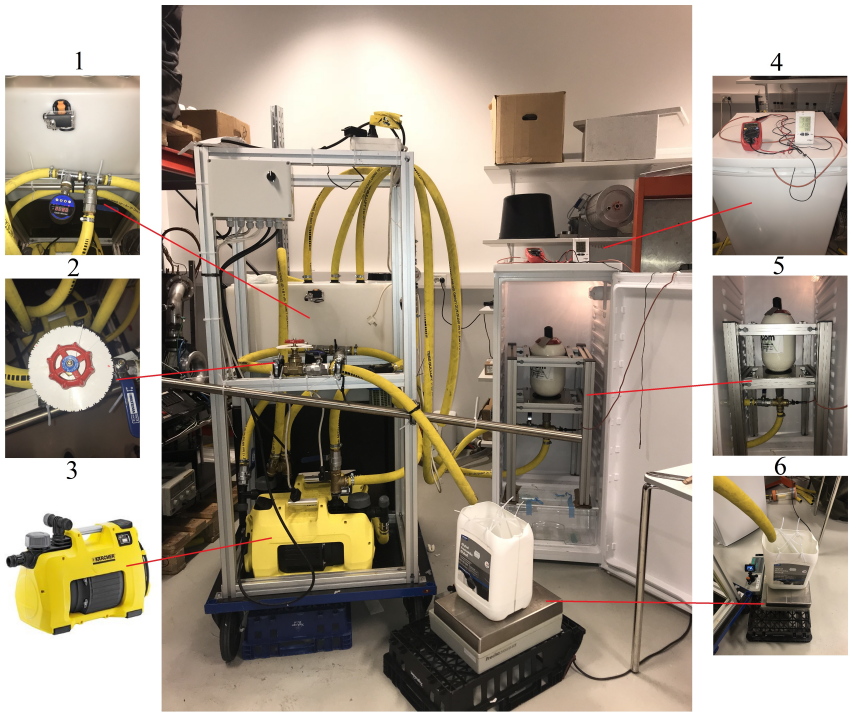

Figure 3.2: The experimental setup

Figure 3.2 shows the setup in its entirety. All the various configurations depicted is further explained in the following sections.

3.2 The accumulator

OneSubsea uses a piston accumulator in their system, but when a bladder type accumulator was donated to the project the decision was made to carry out all experiments with this accumulator type. As has been discovered, literature regarding hydraulic accumulator-testing mainly focuses on piston accumulators, making it even more interesting to discover the behaviour of a less documented configuration.

The accumulator is produced by HYDAC and can be found at their website under the product name SB330-4A1/112U-330A. This accumulator is categorized as a standard bladder accumulator with an inner volume of 4 l and can withstand an operating pressure of 330 bar.

The experimental setup needs to be able to control and monitor the flow of fluid out of the accumulator at a high level of precision. This includes monitoring the pressure, fluid temperature, flow rate and the time it takes to empty the accumulator.

To regulate the flow out of the accumulator, an adjustable gate valve is used. The reason why a gate valve was chosen for this task is that the area of the valve opening has to be known in effort to calculate the discharge coefficient of the valve, which is further discussed in Section 4.2.

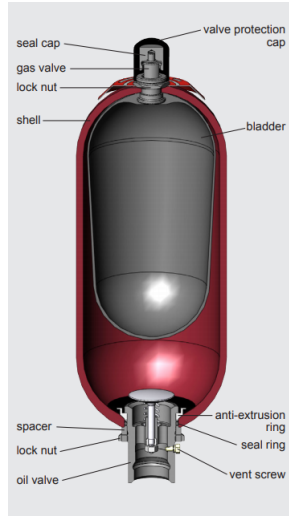

Figure 3.3: Illustration from HyDac's accumulator catalogue

3.3 Determining valve opening

To determine the area of the opening in the valve, the valve gate and opening was drawn in Creo, a 3D CAD software, as can be seen in Figure 3.4a and 3.4c. From this, it was possible to obtain the area of the valve opening for any given gate setting. The gate in the valve is circular with a diameter of 30 mm, while the actual opening in the valve is 26 mm, as shown in Figure 3.4a

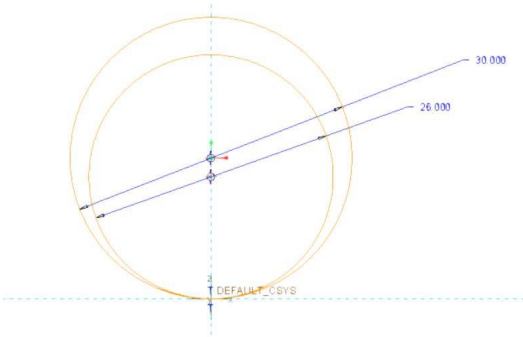

(a) Valve opening and gate drawn in Creo

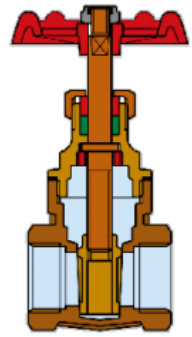

(b) Sketch of the gate valve (Cimberion, 2018)

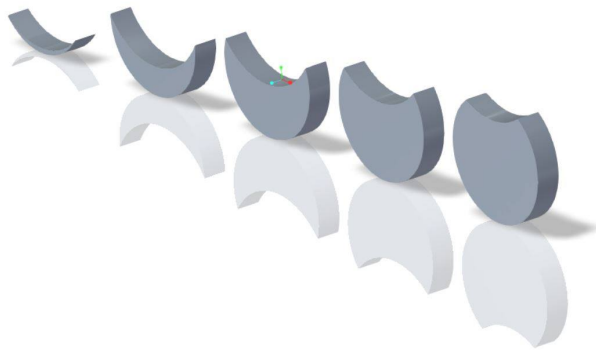

(c) Illustration of valve areas

Figure 3.4: Illustrations from Creo, and sketch from valve producer

The height of the outer stem on the valve does not change when the wheel is turned. This means that the valve opening can't be decided by measuring the stem-height on the outside. As a result, a measuring system depending on the number of turns made on the wheel of the valve had to be made. The number of turns needed to raise the gate 26 mm, i.e. from completely closed to fully opened is 5.25. Meaning that it must be turned a total of 1890°to be opened fully. This means that the gate is raised 1 mm for every $\frac{1890^\circ}{26} = 72.7^\circ$ that the wheel is turned. The solution for determining the number of turns can be seen in Figure 3.5. The "0-mark" on the disc in Figure 3.5 marks the point where the gate is completely closed, and every following notch in the counter-clockwise direction indicates a 10°turn. The disc is connected to the body of the valve making it stationary, while the needle/indicator is connected to the wheel of the valve. When the wheel is turned the needle indicates on the disc how many degrees the wheel has been turned. In Figure 3.5, the wheel is turned to 72.7°, resulting in a gate height of 1 mm.

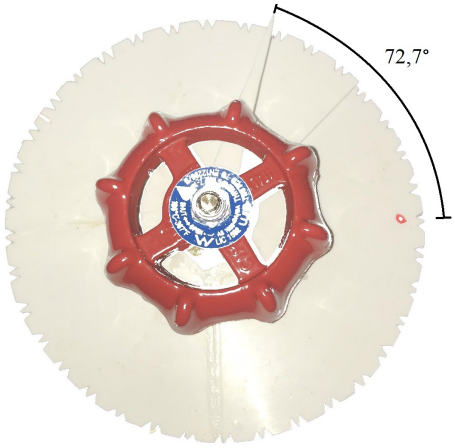

Figure 3.5: System for measuring the valve gate height

3.4 Logging pressure reduction and flow rate in the accumulator

Cameras are used to record the pressure reduction and flow rate in the accumulator. The footage is later logged into a computer manually by using a media player that enables user defined time steps. The two configurations can be seen in Figure 3.6

(a) Recording pressure

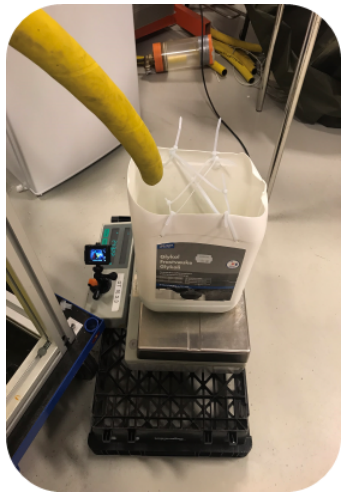

(b) Recording weight of fluid

Figure 3.6: Setup for recording the pressure reduction and flow rate from the accumulator

The pressure is measured by a digital manometer. The flow rate is calculated from the gradually increasing weight of the discharged fluid going into the container placed on top of the scale in Figure 3.6b. The scale is a Precisa 24000 D SCS.

3.5 Temperature measurements

It is desirable to measure the temperature inside the accumulator as well as its surrounding temperature. For the inside temperature measurement, a Pt100 from JUMO depicted in Figure 3.7 is used. The way a Pt100 works, is that the resistance in a platinum element, hence the name Pt, is 100 Ω at 0°C, and increases with 0.385 $\frac{\Omega}{^{\circ}C}$. A multimeter is therefor also needed to determine the temperature measured by the Pt100. It would be beneficial to measure the temperature on the actual inside of the accumulator. This, however, is not a possibility since the accumulator has a bladder and not a piston, where intrusions on the accumulator shell would result in the bladder taking damage or possibly bursting. The next best thing is to place the element as close to the outlet of the tank as possible, which is the solution seen in Figure 3.7. To measure the temperature of the accumulator's environment, a simple temperature measuring device from Clas Ohlson is used. This makes it possible to get an indication of the temperature difference between the inside and outside of the accumulator.

Figure 3.7: Pt100 from JUMO (RS, 1999)

(a) Placement of the Pt100

(b) Multimeter and temperature measurer

Figure 3.8: Multimeter connected to the Pt100 and the temperature measuring device

3.6 Umbilical

Experiments where an actual umbilical system is replicated will also be carried out. The system is the same as what has been described previously. The only difference being that the accumulator will now be connected to a up to 80-meter-long tube and placed in a stairwell at various elevations. The length of the tube can also be altered by means of cutting it.

(a) Accumulator in stairwell

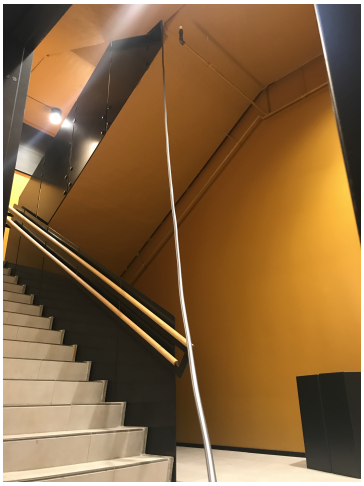

(b) Umbilical decending stairwell

(c) Hallway

(d) Pumps and flow measurement

Figure 3.9: Experimental setup for umbilical tests

Chapter 4

Materials and basic methodology

There are several factors that need consideration before starting the main experiments on the accumulator. The parameters of the fluid in the system needs to be documented, the means of measuring flow rate in the system must be established and various coefficients and constants needs identifying. All of this will be described further in the following sections

4.1 Fluid

HyCom AS, who supplied the accumulator for this thesis has tested it at their facility and used transaqua as hydraulic fluid. In this case they used a water/glycol-mix with a glycol-content of 10 %. The reason for using a glycol-mix is to prevent corrosion inside of the accumulator shell. For the first mixture, 24 l of glycol with an ethylene glycol-concentration of 75 % was purchased from Biltema. The reservoir on the experimental setup will contain 150 l of fluid in total, meaning that 20 l of the glycol-mixture will be needed to achieve 10 % glycol concentration. This results in a mixture containing 20 l of glycol and 130 l of water. For further experiments, several other concentrations will also be mixed and tested. It has been decided that the remaining mixtures will have glycol concentrations of 0, 5, 15 and 20 % respectively.

4.1.1 Density

For future calculations it is necessary to obtain the density of the fluid mixtures. Density of water is set to 1000 $\frac{kg}{m^3}$ while the glycol has a density of 1100 $\frac{kg}{m^3}$, given by the producer. The density of a mixed fluid can be calculated as shown in Equation 4.1 (TETRA, 2005).

$$\rho_{fluid} = \frac{(\rho_{water} V_{water}) + (\rho_{glycol} V_{glycol})}{V_{water} + V_{glycol}} \tag{4.1}$$

As stated above, the mixture will contain 130 l of water and 20 l of glycol. This equals 0.13 m^3 of water, and 0.02 m^3 of glycol, respectively. The resulting density of the fluid becomes 1012.5 $\frac{kg}{m^3}$

The remaining four fluid densities can be seen in Table 4.1

Glycol concentration [%]	Density [$\frac{kg}{m^3}$]
0	1000.00
5	1006.25
15	1018.75
20	1025.00

Table 4.1: Fluid densities at various glycol concentrations

4.1.2 Heat capacity

Alongside the fluid density, the heat capacity of the fluid will have an impact on the experiments on the accumulator due to the temperature changes the accumulator will undergo. Again, this is a mixture of two fluids, making it necessary to calculate the new heat capacity of the fluid post mixture. Teja (1983) suggests a simplified calculation of heat capacity in a fluid mixture. The equation in question can be seen in Equation 4.2.

$$c_p = c_{p1}w_1 + c_{p2}w_2 \tag{4.2}$$

where c_{p1} is the heat capacity of water, c_{p2} the heat capacity of ethylene glycol and w_1 and w_2 are the weight ratios of water and ethylene glycol in the mixture respectively. Below are the ratios for the 10 % glycol concentration

- c_{p1} = 4.187 [$\frac{kJ}{kg \cdot K}$]
- c_{p2} = 2.36 [$\frac{kJ}{kg \cdot K}$]
- w_1 = 87.27 %
- w_2 = 12.63 %

Heat capacities for the five fluids can be seen in Table 4.2.

Glycol concentration [%]	Heat capacity [$\frac{kJ}{kg \cdot K}$]
0	4.187
5	4.072
10	3.952
15	3.839
20	3.721

Table 4.2: Heat capacities for all five fluids

4.1.3 Viscosity

The viscosity in a fluid is a measurement of its resistance to shear, or in other words, its resistance to flow. High viscosity indicates high resistance to flow while low viscosity implies low resistance. Viscosity is very pressure and temperature dependent making it an important parameter for the experiments.

Thanks to the chemistry department at Western Norway University of Applied Sciences, it was possible to determine the viscosity of the five fluid samples using their falling sphere rheometer. The results provided can be seen in Table 4.3

Concentration [%]	**Viscosity [mPa·s]**
0	1.106
5	1.258
10	1.474
15	1.745
20	2.033

Table 4.3: Viscosity of the fluid samples sent to the chemistry lab at Western Norway University of Applied Sciences

4.2 Discharge coefficient

The discharge coefficient refers to the ratio of the actual discharge to the theoretical discharge in a turbulent nozzle. This coefficient will be used to verify experimental results up against those retrieved from analytical work done in a previous project (Hiis and Stenhjem, 2017). The coefficient can be found experimentally. Equation 4.3, which has been presented in Section 2.4 for general cases, can be used to obtain the discharge coefficient.

$$Q = \hat{\mu} \cdot A_{valve} \cdot \sqrt{\frac{2 \cdot \Delta P}{\rho}} \tag{4.3}$$

The parameters of Equation 4.3 are as follows:

- $\hat{\mu} =$ Discharge coefficient of a pre-set valve orifice
- $A_{valve} =$ The area of the pre-set valve orifice
- $\rho =$ Fluid density
- $\Delta P =$ The pressure loss over the valve

The hydraulic circuit used to determine $\hat{\mu}$ can be seen in Figure 4.1

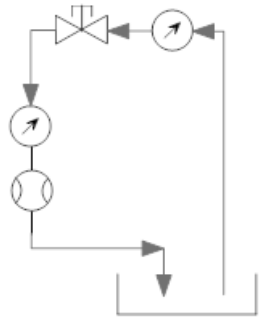

.

Figure 4.1: Experimental setup to acquire the discharge coefficient $\hat{\mu}$

The valve openings that were chosen for the full length of the project can be seen below

Valve openings		
Valve setting	**[mm^2]**	**[m^2]**
1	2.53	$2.53 \cdot 10^{-6}$
2	6.80	$6.80 \cdot 10^{-6}$
3	11.90	$11.90 \cdot 10^{-6}$
4	15.40	$15.40 \cdot 10^{-6}$
5	38.10	$38.10 \cdot 10^{-6}$

Table 4.4: Areas of specific valve settings

To obtain the flow rate through the valve, a simple water counter was utilized. The system ran for two minutes for each valve opening. Meaning that the valve gate was first raised to a valve opening of 2.53 mm^2 and held there for 2 minutes. The pressure loss over the valve and the amount of fluid that had travelled through it was noted before the exact same thing was done for the remaining four openings.

Discharge Coefficients 10 % concentration	
Valve opening [mm^2]	$\hat{\mu}$
2.53	0.563
6.79	0.584
11.90	0.591
15.44	0.646
38.10	0.768

Table 4.5: Discharge coefficients for the five valve openings at a 10 % glycol concentration

When using measuring devices, there will always be a level of uncertainty in the readings. It is possible to calculate the error propagation of components, which has been done

for the water counter. Equation 4.4 is the general function for error propagation where the flow (Q) is a function of velocity (v) and time (t). σ_sV and σ_st is the true standard deviation of the volume and time respectively

$$\partial Q = \sqrt{(\frac{\partial Q}{\partial V})^2 \sigma_s V^2 + (\frac{\partial Q}{\partial t})^2 \sigma_s t^2} \tag{4.4}$$

$$Q = \frac{V}{t} \qquad \frac{\partial Q}{\partial V} = \frac{1}{t} \qquad \frac{\partial Q}{\partial t} = \frac{V}{t^2}$$

In this case, the timer used to measure the time steps of one second is considered to be free of uncertainty, meaning that σt is 0. This results in the final equation for error propagation for the water counter

$$\partial Q = \sqrt{\sigma_s V^2} = \sigma_s V \tag{4.5}$$

This has been calculated through multiple experimental tests

Test number (i)	Volume [l]	$\Delta\overline{\text{volume}}$ [l]	$(\Delta\overline{\text{volume}})^2$
1	0.850	0.0675	$4.56{\cdot}10^{-9}$
2	0.825	0.0425	$1.81{\cdot}10^{-9}$
3	0.760	-0.0225	$5.06{\cdot}10^{-10}$
4	0.700	-0.0825	$6.81{\cdot}10^{-9}$
5	0.795	0.0125	$1.56{\cdot}10^{-10}$
6	0.755	-0.0275	$7.56{\cdot}10^{-10}$
7	0.775	-0.0075	$5.62{\cdot}10^{-11}$
8	0.800	0.0175	$3.06{\cdot}10^{-10}$

Table 4.6: Data from tests carried out on the water counter used to determine accumulator flow

The sum of diff from mean is $1.495{\cdot}10^{-8}$ and is denoted as x_m. Now the true standard deviation for volume can be calculated as shown:

$$\sigma_s V = \sqrt{\frac{x_m}{i-1}} \tag{4.6}$$

giving a standard deviation of $\pm 4.62 \cdot 10^{-5}$, which is quite a substantial error considering the mean volume over 1 second is $7.825{\cdot}10^{-4}$ and gives an error propagation of $\pm$ 5.9 %.

4.3 Determining the thermal time constant

When carrying out experiments on the accumulator, the temperature of the fluid is an important parameter to consider as it will have an impact on the gas in the bladder. It is of interest to have the same temperature both inside and outside of the accumulator before

initiating the discharge. To achieve this, the thermal time constant of the system needs to be derived. To determine the thermal time constant for the accumulator, a thermometer will measure both the inside temperature of the accumulator, as well as the temperature of the room where the accumulator is placed.

As mentioned earlier, the thermal time constant can be found with Equation 2.31. The value of the parameters in the equation are as follows:

- ρ = 1012.5 [$\frac{kg}{m^3}$]
- c_p = 3.952 [$\frac{kJ}{kg \cdot K}$]
- $V_{discharge}$ = the volume of fluid in the accumulator at full charge [m^3]
- h = 11.3 [$\frac{W}{m^2 \cdot K}$] (Toolbox, 2003b)
- A_s = The total surface area that the fluid touches in the accumulator [m^2]

To calculate A_s, the total surface area of the inside of the accumulator shell needs to be found. Figure 4.2 shows dimensions provided by HyDac.

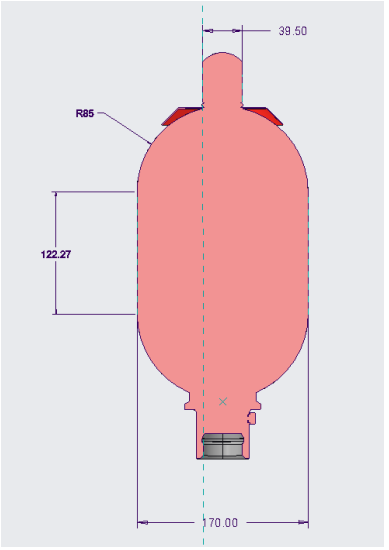

Figure 4.2: Dimensions of the accumulator from HyDac's web page

The total surface area of the accumulator shell is approximately

$$A_{accumulator} = (h\pi D) + (4\pi\left(\frac{D}{2}\right)^2) \tag{4.7}$$

Knowing that the total volume of the accumulator, $V_{accumulator}$, is 4 l, it is possible to approximate A_s when the volume of the fluid inside the accumulator, $V_{discharge}$, is known

$$A_s = A_{accumulator} \cdot \frac{V_{discharge}}{V_{accumulator}} \tag{4.8}$$

$A_{accumulator}$ was found to be 0.1561 $[m^2]$ from Equation 4.7 and $V_{discharge}$ 2.5 l from section 4.4. Using the results, A_s = 0.0908 m^2 and τ = 9613.39 s.

The thermal time constant of the gas is also of interest as it will give an indication of what to expect in terms of rate of internal energy loss. The parameters used for these calculations are given below.

- ρ = 1.276 $[\frac{kg}{m^3}]$
- c_p = 1.006 $[\frac{kJ}{kg \cdot K}]$(Toolbox, 2003a)
- h = 7.9 $[\frac{W}{m^2 \cdot K}]$ (Toolbox, 2003b)

4.4 Validating analytical approach to accumulator discharge

From previous studies (Hiis and Stenhjem, 2017), an analytical approach to an accumulator's behaviour regarding pressure reduction during discharge has been developed. Equation 4.9 is the resulting equation from the studies, and will be validated experimentally.

$$P(t) = \left(\frac{1}{\frac{\beta t(\gamma+2)}{2\alpha} + P_o^{-\frac{\gamma+2}{2\gamma}}} \right)^{\frac{2\gamma}{\gamma+2}} \tag{4.9}$$

- P_o = Pressure in the bladder when the accumulator is filled with fluid
- V_o = Volume of the gas in the bladder when the accumulator is filled with fluid
- $\beta = A_{valve} \cdot \hat{\mu} \cdot \sqrt{\frac{2}{\rho}}$
- $\alpha \Rightarrow P_o \cdot V_o^{\gamma} = C \Rightarrow V_o = \frac{C^{\frac{1}{\gamma}}}{P_o^{\frac{1}{\gamma}}} \Rightarrow C^{\frac{1}{\gamma}} = \alpha$
- γ = 1.4

For the flow rate out of the accumulator, Equation 4.3 is used by inserting Equation 4.9 as ΔP

V_o was found experimentally by discharging the accumulator until it was completely empty, making it possible to estimate the volume of the compressed gas. Seeing how the accumulator has a pre-charge pressure of two bars, it is easy to assume that the accumulator will be completely empty at 2 bars as well. This is not the case however. The gas in the bladder will undergo a rapid pressure reduction upon discharge (adiabatic process), resulting in a big temperature difference between the gas and its surroundings. Due to the low temperature, once fully discharged, the pressure in the bladder will be even lower than that of the pre-charge pressure before the temperature in the gas evens out with its surroundings, i.e. increases corresponding to the temperature. The volume of fluid in the accumulator was 2.5 l, meaning that the volume of the gas when compressed is 1.5 l.

The smallest valve opening (2.53 mm^2) was tested first, where P_o = 8.78 bars. The pressure reduction as a function of time for both the analytical solution and the experimental test can be seen in Figure 4.3a. The results in Figure 4.3a are quite good, and is a strong indication that the analytical solution is valid. However, as stated above, tests were also done for much larger valve openings, resulting in a more rapid reduction in the pressure in the accumulator, as can be seen in Figure 4.3c. As the valve opening is increased even further, as in Figure 4.3e, the resolution of the manometer turns out to be too low to give a good reading. The reduction in pressure is of such a magnitude the first 1.5 seconds of discharge that the resolution of the manometer seems insufficient.

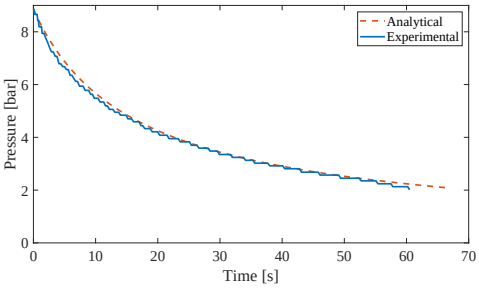

(a) P(t) for 2.53mm^2 valve opening

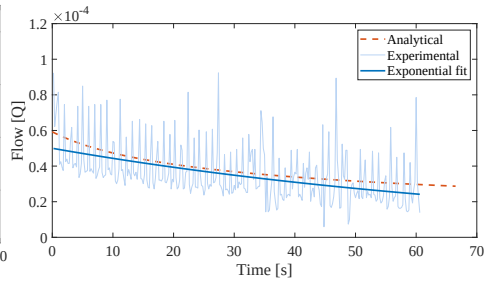

(b) Q(t) for 2.53mm^2 valve opening

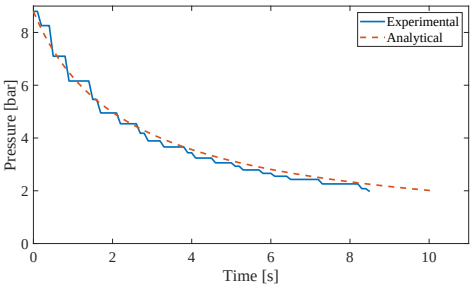

(c) P(t) for 15.44mm^2 valve opening

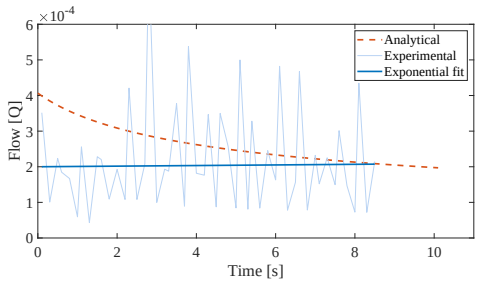

(d) Q(t) for 15.44mm^2 valve opening

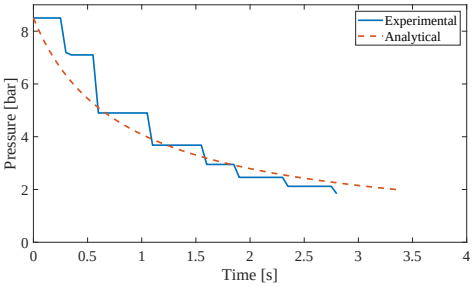

(e) P(t) for 38.1mm^2 valve opening

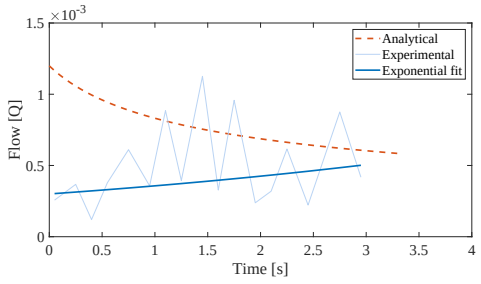

(f) Q(t) for 38.1mm^2 valve opening

Figure 4.3: Experimental results against analytical solution

Chapter 5

Experiments

The scope of the experiments in this thesis is to investigate the influence temperature, precharge and viscosity of the hydraulic fluid has on a hydraulic accumulator's performance, and through these findings shed some light on possible reasons why OneSubsea is experiencing their rapid initial pressure reduction. The working theory for the experiments is that the compressed gas is going through an adiabatic process at discharge due to its rapid nature. Even though OneSubsea's accumulators more than likely are going through an isothermal process due to flow rates as low as 0.5 $\frac{l}{h}$, it is of interest to investigate the accumulators adiabatic behaviour. This enables more experiments to be carried out in a shorter time span, and the various conditions the accumulator is exposed to will yield results regardless of the thermodynamic process. Additional tests with drastically lower flow rates to achieve isothermal process will also be carried out.

When it comes to uncertainties in the experimental data, there are several aspects that need consideration. As explained previously, the water counter used to determine the discharge coefficients of the valve, has quite a substantial level of uncertainty. The digital manometer and scale used to measure pressure and flow rate will also have levels of uncertainty. The pressure levels supplied by the two pumps in the system has varied in a range of 8.6 to 8.9 bars. This however, is not considered a problem seeing how the analytical solution used to validate the experiments is able to take these variations in initial pressure into account.

Equipment	Uncertainty
Water counter	$\pm$5.9 %
Manometer	$\pm$0.5 %
Precisa scale	$\pm$0.2 g

Table 5.1: Uncertainties of equipment in the experimental setup

All experiments have been carried out at the hydraulics lab at the Western Norway University of Applied Sciences

5.1 Establishing the standard conditions

For the experiments, a set of values are chosen to be considered as standard conditions. The temperature in the lab is 20°C, the pre-charge pressure in the bladder is 2 bars and the pressure when the accumulator has been filled with fluid is approximately 8.8 bars. From Section 4.4 it is clear to see that the analytical solution is quite accurate, especially when considering the smallest valve opening (2.53 mm^2). Because of this, the 2.53 mm^2 valve opening will also be considered as a standard condition.

With these standard conditions in mind, a base case branching out to different alterations in condition has been developed. Table 5.2 describes the plan for the experiments.

Pre-charge [bar]	**A$_{valve}$ [mm^2]**	**T$_{accumulator}$ [°C]**	**Glycol concentration [%]**
2 3 4 5	2.53	20	10
2	6.80 11.90 15.44 38.10	20	10
2	2.53	43.00 10.38 9.35 -4.93 5.71	10
2	2.53	20	0 5 15 20

Table 5.2: The planned experiments listed

5.2 Various valve openings

Simple test for various valve openings are carried out to further strengthen the analytical solution.

5.3 Altering temperatures

The next step in the proceeding experiments is to reduce and increase the temperature of the accumulator. A refrigerator will be used to lower the temperature and a heating fan will increase the temperature. The reason why this is of interest is that the internal energy of the gas in the accumulator is greatly affected by heat both leaving and entering the gas in the bladder.

When the accumulator is filled with fluid and the gas is compressed, the temperature in the gas increases together with its internal energy. Once the accumulator is fully charged with hydraulic fluid, the gas will start cooling down due to natural convection to the accumulator shell and radiation from the accumulator shell to its surroundings. The fluid filling the accumulator has an initial temperature of 20°C and needs time to even out with the decreased surrounding temperature. The thermal time constant of the hydraulic fluid will be much greater compared to that of the gas due to the difference in density, and the fluid will therefore also delay the cooling of the gas once discharge has been initiated and the gas expands. The accumulator is not re-pressurized after being cooled down. The reason for this being that this would result in increased temperatures in the accumulator due to the gas in the bladder being re-compressed and "new" uncooled hydraulic fluid could potentially enter the tank. This would require a new period of cooling to equalize the internal temperature with that of the surroundings. Furthermore, this would again result in a pressure reduction in the bladder, and nothing will have changed for what conditions are concerned. An increase in surrounding temperature will result in increased internal energy in the form of heat in the gas. The first test carried out with setting 1 on the refrigerator for example, has an initial pressure and temperature of 8.6 bars and 20°C, respectively. Using Gay-Lussac's law, the corresponding constant C becomes $\frac{8.6bars}{294.15K} = 0.02933$

Setting 1 on the refrigerator gives a temperature inside the accumulator of 10.38°C. This should, according to Gay-Lussac's law, result in 8.317 bars of pressure in the accumulator. The actual pressure measured in the accumulator was 8.32 bars, which will in this case be considered coinciding results.

Three temperature settings for the refrigerator has been chosen for the experiments. The corresponding temperatures at the inlet of the accumulator is given in Table 5.3

Setting in refrigerator	$\mathbf{T}_{accumulator}$
0	20.00°C
1	10.38°C
4	9.35°C
7	-4.93°C

Table 5.3: Temperature in the refrigerator at given settings

It is desirable to increase the temperature of the accumulator's surroundings as well. The refrigerator is turned off and a heater fan is placed inside. The heater is set to keep the temperature between 48 and 56°C. The reason for this fluctuation in temperature is the thermostat that is built in to the heater and its precision. This makes it difficult to even out the temperatures in the accumulator and its surroundings. This will be discussed in more detail in the following section.

5.4 Discharge while undergoing natural convection

For this section of the experiments, the effects on the accumulator discharge while the accumulator is undergoing cooling or heating, or in other words, when natural convection occurs, will be investigated.

The way to determine the possible effects of the accumulator undergoing cooling or heating is to initiate discharge before the internal and external temperatures have equalled out. For these experiments, only 30 % of the necessary cooling/heating-time, determined from the data presented in Section 4.3, will pass before discharging in an effort to still have the accumulator undergo natural convection. The data for the cooling experiment can be seen in Table 5.4.

Valve opening	2.53 mm^2
Refrigerator setting	7
Temperature of accumulator	5.71°C
Time waited	4.07 hours

Table 5.4: Parameters for cooling-test

As previously stated, tests where the accumulator is undergoing heating will be described in this section due to difficulties related to keeping the temperature at a steady level. The heat level will be kept between 48 and 56°C, and the time given for the accumulator to heat up is also here set to 30 % of what is calculated from Equation 2.31 put into Equation 2.33. Table 5.5 shows the data for the heating experiment of the accumulator.

Figure 5.1: The heating fan used

Valve opening	2.53 mm^2
Temperature of fluid	43°C
Time waited	4.3 hours

Table 5.5: Parameters for heating-test

5.5 Change in pre-charge pressure

To get a better understanding of how the initial conditions in the accumulator affects its performance, the pre-charge pressure in the accumulator will be altered. For the experiments, the pre-charge will be increased to 3, 4 and 5 bars. By conducting these experiments, it will be possible to determine if a reduction in compression rate will either increase, decrease or not change the rate at which fluid is discharged from the accumulator.

It will be interesting to look at the different pre-charges whether the reduction in pressure from 8.8 bars to the given pre-charge will happen at the same rate as when the pre-charge pressure is at 2 bars, or if the discharge will follow the analytical solution, which is pictured in Figure 5.2

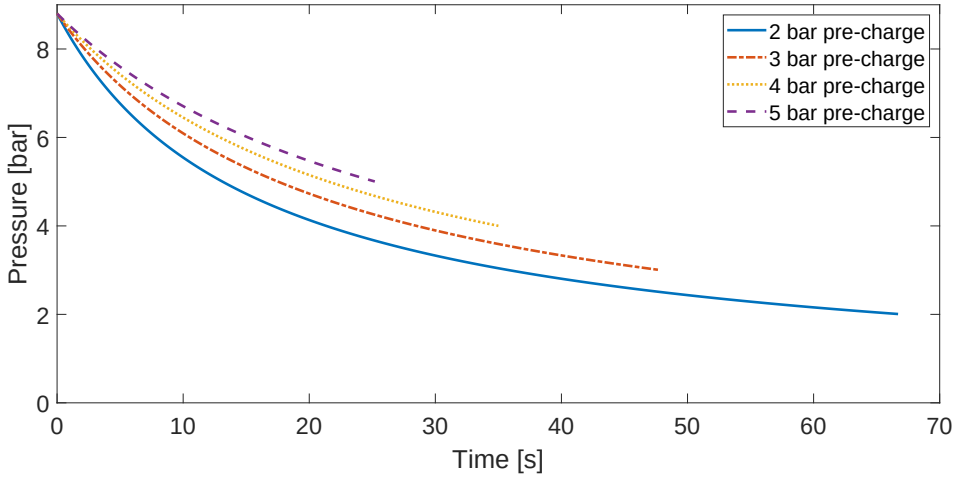

Figure 5.2: Analytical solutions for the four pre-charge settings

5.6 Change in glycol concentration

The amount of glycol in the fluid will be altered. The reason for doing this is that it will change the viscosity and density of the fluid which is expected to have an impact on the results from discharging the accumulator.

5.7 Umbilical tests

After having identified all the mentioned effects on the accumulator in a simplified environment regarding pipe length, an imitation of OneSubsea's umbilical-system is tested. The system is not to different from that of the other tests. The only differences are that the accumulator is connected to the rest of the setup by first a 40 and later an 80-meter-long tube. The Pt100 has been removed, as the temperature of the fluid is no longer being investigated, and the digital manometer has been installed in its place. A second, analogue manometer is now installed where the digital manometer was initially installed. The reason for this begin that all tests will now have had the same manometer installed at the entrance to the accumulator, and the same levels of uncertainty will apply to all the tests.

5.8 Isothermal process

A simple experiment where the goal is to recreate the accumulator behaviour that OneSubsea is witnessing will be carried out. The real accumulator system has a total discharge time of approximately 4 hours. This, as mentioned earlier, will most likely involve an isothermal process during discharge. To be able to recreate these conditions, a drastic decrease in fluid flow from the test-accumulator is needed. The gate valve is in this case practically closed, and the only flow that passes through the valve can be described as leakage.

Chapter 6

Results and Discussion

6.1 Various valve openings

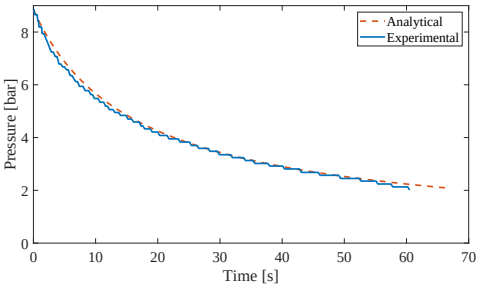

(a) P(t) for 253mm^2 valve opening setting 0

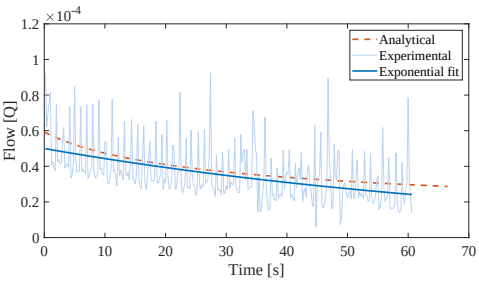

(b) Q(t) for 253mm^2 valve opening setting 0

Figure 6.1: 2.53 mm^2 valve orifice

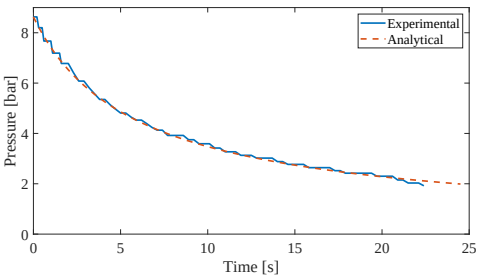

(a) P(t) for 680mm^2 valve opening setting 0

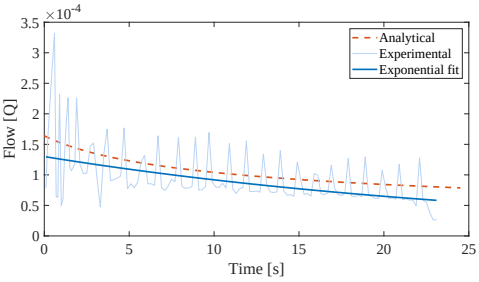

(b) Q(t) for 6.80mm^2 valve opening setting 0

Figure 6.2: 6.80 mm^2 valve orifice

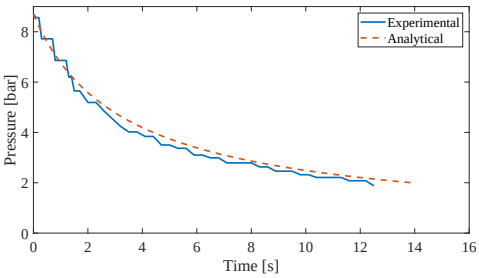

(a) P(t) for 11.90mm^2 valve opening setting 0

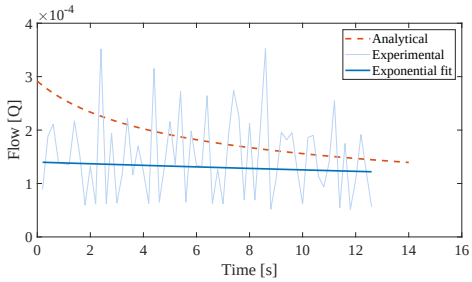

(b) Q(t) for 11.90mm^2 valve opening setting 0

Figure 6.3: 11.90 mm^2 valve orifice

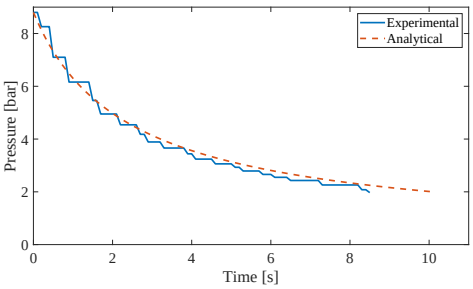

(a) P(t) for 15.4mm^2 valve opening setting 0

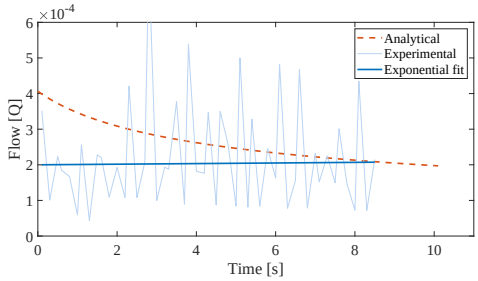

(b) Q(t) for 15.4mm^2 valve opening setting 0

Figure 6.4: 15.40 mm^2 valve orifice

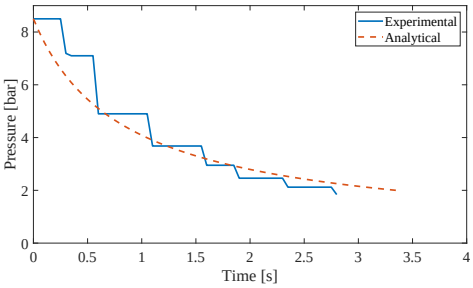

(a) P(t) for 38.1mm^2 valve opening setting 0

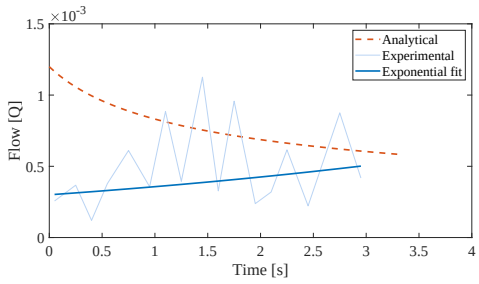

(b) Q(t) for 38.1mm^2 valve opening setting 0

Figure 6.5: 38.10 mm^2 valve orifice

6.2 Altering temperatures

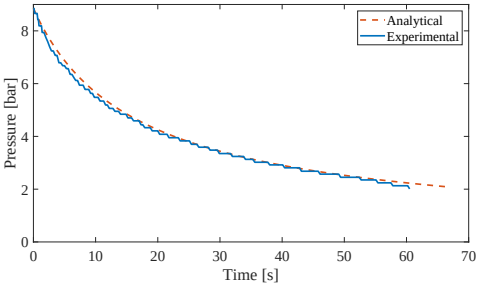

(a) P(t) for 2.53mm^2 valve opening setting 0

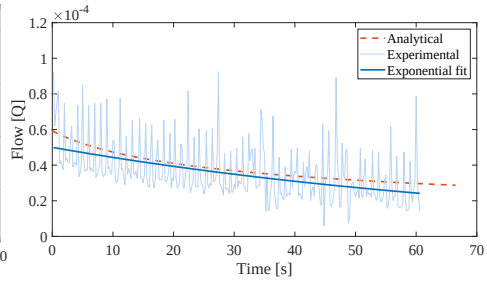

(b) Q(t) for 2.53mm^2 valve opening setting 0

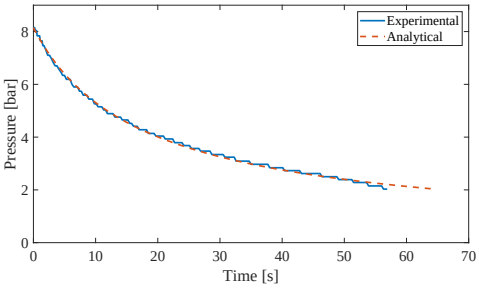

(c) P(t) for 2.53mm^2 valve opening setting 1

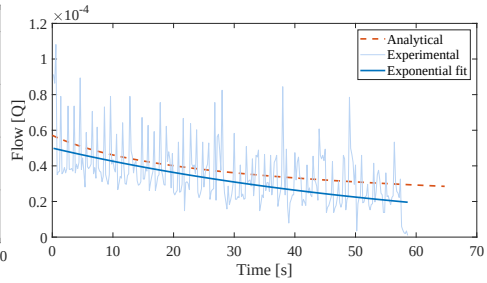

(d) Q(t) for 2.53mm^2 valve opening setting 1

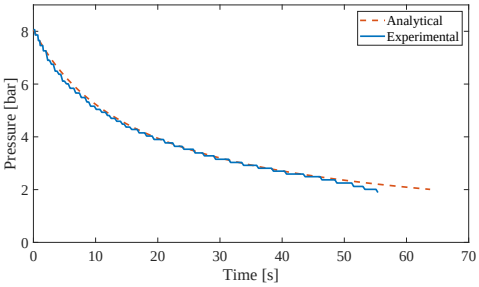

(e) P(t) for 2.53mm^2 valve opening setting 4

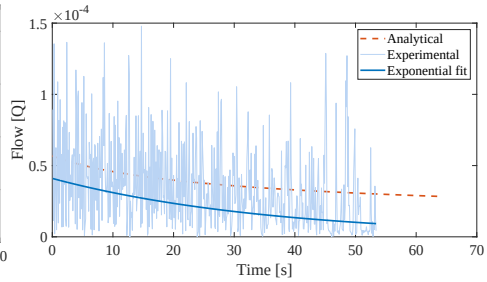

(f) Q(t) for 2.53mm^2 valve opening setting 4

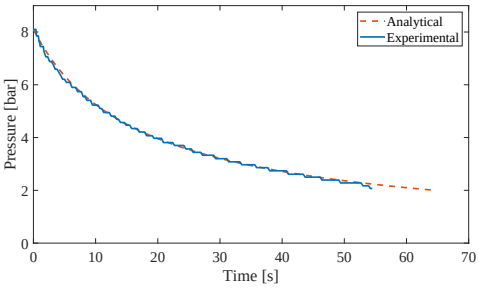

(g) P(t) for 2.53mm^2 valve opening setting 7

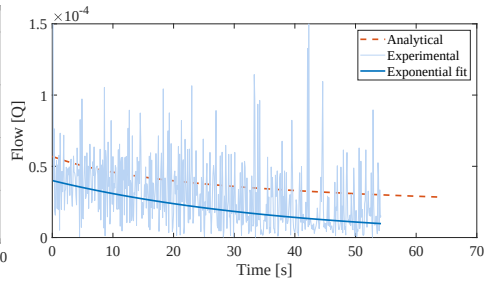

(h) Q(t) for 2.53mm^2 valve opening setting 7

Figure 6.6: Experimental results against analytical solution for altered temperature

The discrepancies between the experimental and the analytical solution can be calculated using Equation 6.1

$$\delta = \frac{P_{experimental} - P_{analytical}}{P_{analytical}} \tag{6.1}$$

Where δ is the discrepancy, $P_{experimental}$ is the pressure from the experiments and $P_{analytical}$ is the pressure given by the analytical solution The discrepancies for the four cooling-experiments are given in table 6.1

Temperature setting	Average discrepancy [%]	Maximum discrepancy [%]
0	1.60	9.30
1	1.95	8.31
4	2.29	16.69
7	1.36	8.43

Table 6.1: Discrepancies with respect to pressure for temperature alteration

Temperature [°C]	Discharge time [s]
20.00	60.5
10.38	56.9
9.35	55.4
-4.93	54.5

Table 6.2: Discharge times compared to accumulator temperature

It is evident that reduced temperatures in the accumulator's surroundings influences the energy stored in the tank, or more precisely in the gas. The most notable change is the reduction in total pressure in the system. This results in a decreased time where the accumulator can deliver fluid to the system before reaching its pre-charge. As can be seen in Table 6.1 the average deviation between the experimental and analytical results are all below 2.3 %. The maximum discrepancies are on the other hand more substantial. The reason for this is that the pressure in the accumulator is close to the pre-charge pressure, resulting in a reduced "push" from the bladder to the fluid. This is further discussed in Section 6.6. The analytical solution depicts an even push throughout the discharge and does not consider the effect of the accumulator being nearly empty.

The results from reducing temperatures are not unexpected. The system and its surroundings has been given enough time to even out their temperatures, making the results like that of the first tests where the system and its surroundings were held at room temperature.

As mentioned earlier, Gay-Lussac's law is quite accurate in estimating the final pressure of the pressurized system after having experienced thermal losses or gains. Table 6.3 describes the thermal losses in the accumulator and how well Gay-Lussac's law corresponds to the experimental findings

$\mathbf{T}_{accumulator}$[°C]	$\mathbf{P}_{initial}$ [bar]	$\mathbf{P}_{final}$ [bar]	$\mathbf{P}_{theory}$[bar]
10.38	8.50	8.15	8.19
9.35	8.45	8.06	8.11
-4.93	8.55	8.10	8.11

Table 6.3: Gay-Lussac's law against experimental results for altered temperatures

The reason why the pressure in the accumulator at -4.93°C is the same as at 9.35°C according to Gay-Lussac's law is that the accumulator was cooled from 9.35 to -4.93°C instead of having the accumulator regain heat corresponding to the temperature of the room (20°C)

As explained in the Section 5.3, the heating fan could not keep a steady temperature, and could therefor only be used in the natural convection tests. This however is not of great concern seeing how it was proven that thermal equilibrium makes little difference regarding discharge, apart from changing the internal energy of the gas. As a result, the tests where the accumulator is heated will be documented in the next section.

6.3 Natural convection

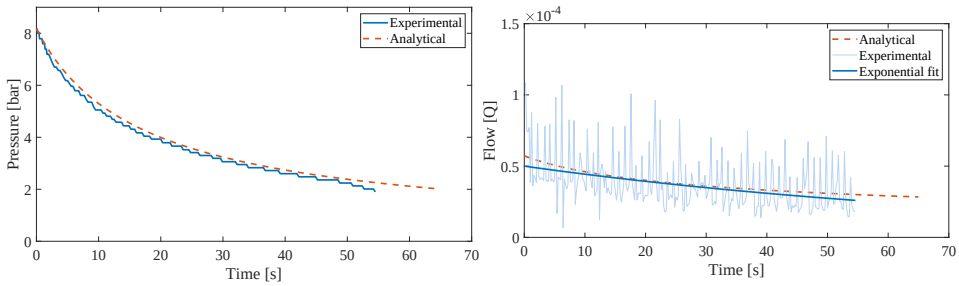

(a) P(t) for setting 7 while undergoing natural convection **(b)** Q(t) for setting 7 undergoing natural convection

Figure 6.7: Experimental results for natural convection (cooling)

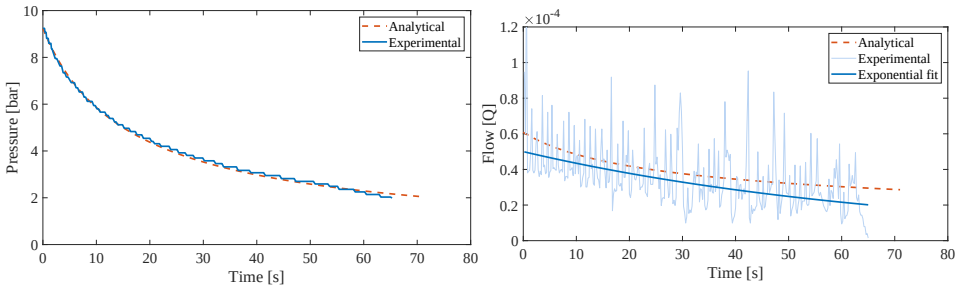

(a) P(t) while undergoing heating

(b) Q(t) while undergoing heating

Figure 6.8: Experimental results for natural convection (heating)

The initial pressure in the accumulator before discharge is, as expected, higher that what it originally was due to the energy that is supplied to the gas in form of heat. This also enables the accumulator to supply fluid over a longer duration of time due to the increased energy in the bladder. The nature of the discharge is still considered adiabatic due to how well the analytical solution corresponds with the experimental results in Figure 6.8. The data for the heating experiment can be seen in Table 5.5

It is quite clear to see from the two experiments that the nature of the accumulator doesn't change with respect to what is expected from the analytical solution. The discrepancy for the experiments are shown below.

Temperature setting	Average discrepancy	Maximum discrepancy
7	4.30 %	18.40 %
Heating	2.14 %	5.31 %

Table 6.4: Discrepancies with respect to pressure when undergoing natural convection

Fluid viscosity and density is influenced by temperature and pressure. The analytical solution that has been used throughout all experiments does not take temperature or fluid viscosity into account, but it does depend on the fluid density. What can be observed from the results obtained from both the heating and cooling-experiments is that the total influence in fluid viscosity and density due to temperature alterations has not given experimental results straying far from that of the analytical solution. Figure 6.7a and 6.8a show small discrepancies between the experimental and analytical results. The difference is however opposite to what would be expected if the increased/decreased temperature influenced the viscosity and density to a great extent. Increased temperature results in decreased viscosity, meaning reduced shear rate against the accumulator and pipe walls, while decreased temperatures would mean the exact opposite. The discrepancies are on such a minuscule level that it is concluded that temperature wouldn't be of great concern regarding fluid flow during adiabatic process. The energy loss or gain depending on whether the accumulator is heated or cooled on the other hand, will influence operation greatly.

$\mathbf{T}_{accumulator}$[°C]	$\mathbf{P}_{initial}$ [bar]	$\mathbf{P}_{final}$ [bar]	$\mathbf{P}_{theory}$[bar]
43.00°C	8.6	9.24	9.27
5.71°C	8.6	8.17	8.15

Table 6.5: Gay-Lussac's law against experimental results for natural convection

6.4 Altered pre-charge

A result of increasing the pre-charge of the accumulator is that the gas is given a permanent increase in internal energy. Further, this reduces the capacity of the accumulator with regards to the amounts of fluid that the tank can store when the maximum pressure from the pumps is approximately 8.8 bars. All together this will give increased flow rates and reduced dis-charge durations as is evident in Figure 6.9. It becomes clear that the analytical equation is less accurate at decreased compression rates. In previous tests, the pressure in the accumulator has had a more rapid decrease once nearing its pre-charge pressure. These tests further illustrate this phenomenon as the pressure decrease in the experiment is straying further and further from the analytical solution as the pre-charge is increased, or in other words, as the pressure at the starting point of discharge is closer to the pre-charge of the accumulator. All in all, Table 6.6 shows discrepancies quite similar to those of the previous results.

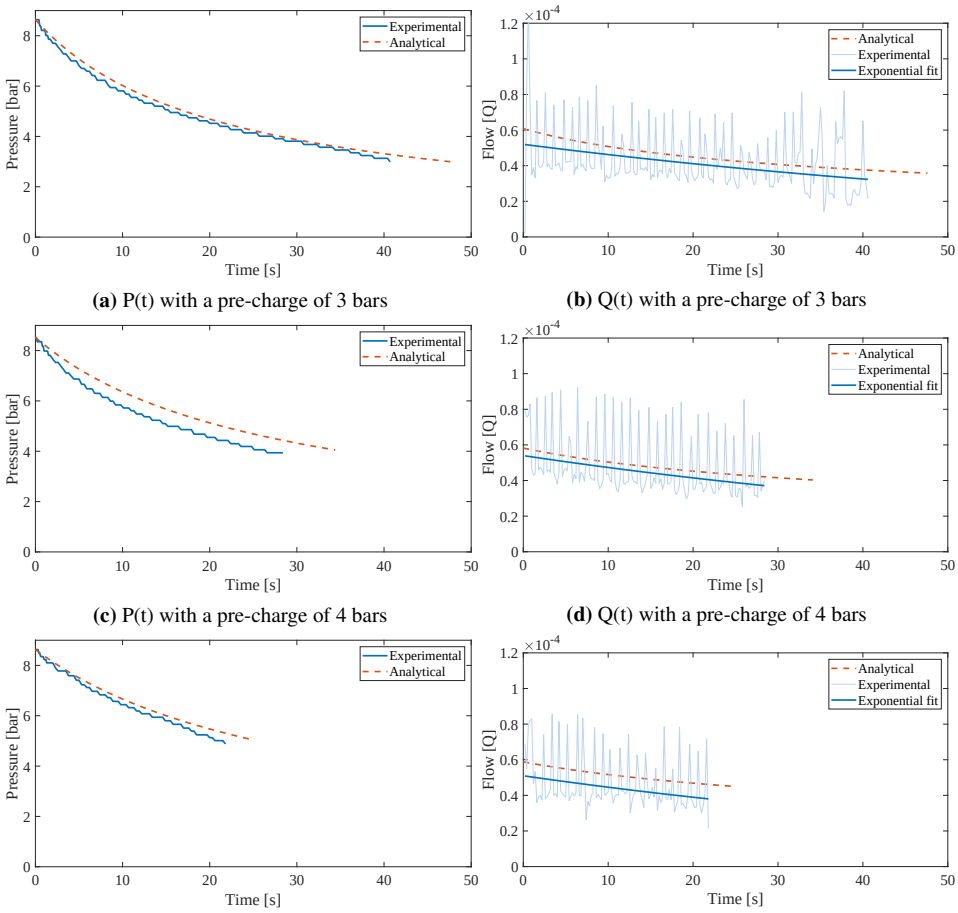

(a) P(t) with a pre-charge of 3 bars

(b) Q(t) with a pre-charge of 3 bars

(c) P(t) with a pre-charge of 4 bars

(d) Q(t) with a pre-charge of 4 bars

(e) P(t) with a pre-charge of 5 bars

(f) Q(t) with a pre-charge of 5 bars

Figure 6.9: Experimental results for 3, 4 and 5 bars of pre-charge

Pre-charge [bar]	Average discrepancy [%]	Maximum discrepancy [%]
3	3.31	9.75
4	4.53	12.08
5	3.11	8.75

Table 6.6: Discrepancies with respect to pressure for the varying pre-charges

6.5 Change in glycol-concentration

It is evident that the increase in fluid viscosity has great impact on the shear rate between the fluid and the pipe walls. The increase from 0 % to 5 % concentration does not do too much for what increased time of discharge is concerned. It is first at 15 % concentration

that the impact becomes clear. Table 6.7 shows an exponential increase in time needed to discharge the accumulator as the concentration rises. Table 6.8 shows that the viscosity does not change linearly with the concentration either, but also has an exponential increase as the concentration rises. A correlation between the discharge time and viscosity of the fluid is identified.

Concentration [%]	**Discharge time [s]**	**Discharge increase (0 to x%) [%]**
0	59.6	0.0
5	59.9	0.5
10	60.5	1.5
15	62.0	4.0
20	67.4	13.0

Table 6.7: Discharge times compared to percentage of glycol in the fluid

Concentration [%]	**Viscosity [mPa·s]**	**Viscosity increase (0 to x%) [%]**
0	1.106	0.00
5	1.258	13.74
10	1.474	33.27
15	1.745	57.77
20	2.033	83.81

Table 6.8: Discharge times compared to percentage of glycol in the fluid

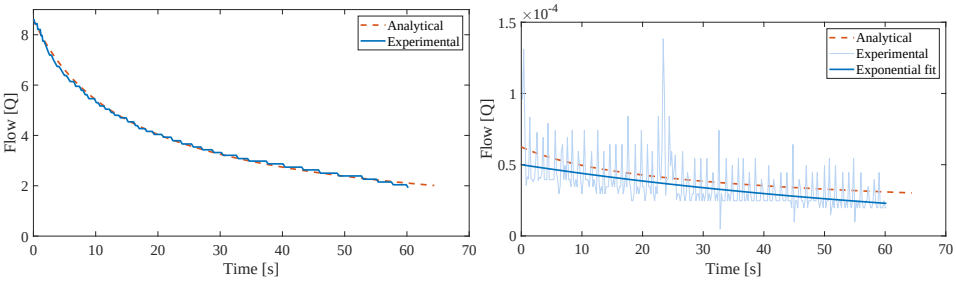

(a) P(t) with 0 % glycol in the fluid

(b) Q(t) with 0 % glycol in the fluid

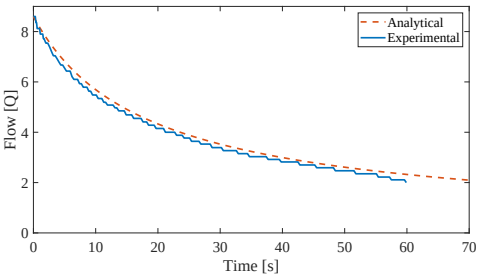

(c) P(t) with 5 % glycol in the fluid

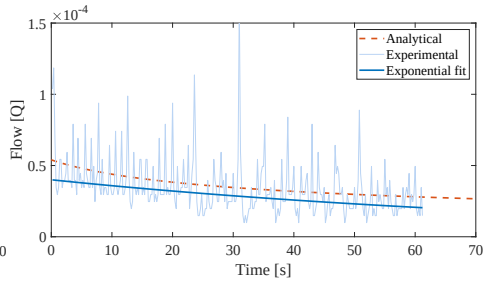

(d) Q(t) with 5 % glycol in the fluid

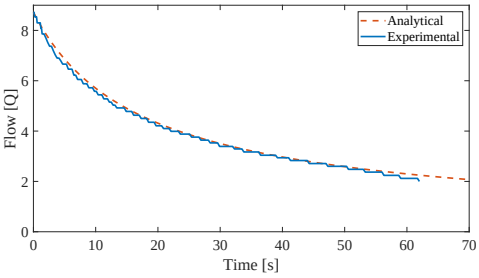

(e) P(t) with 15 % glycol in the fluid

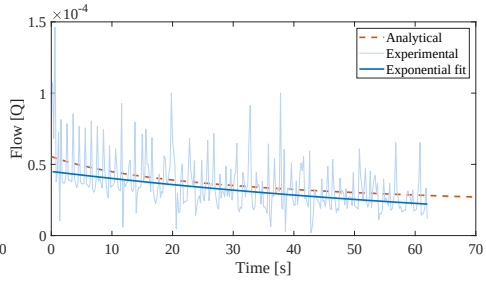

(f) Q(t) with 15 % glycol in the fluid

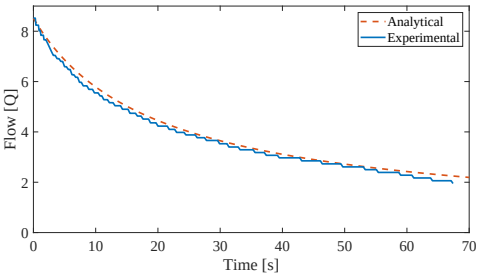

(g) P(t) with 20 % glycol in the fluid

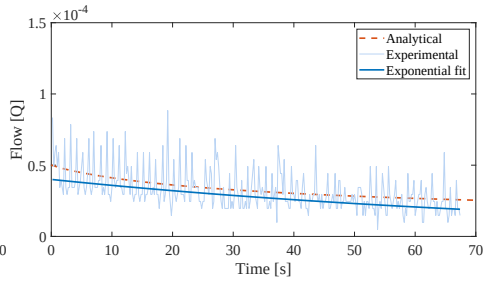

(h) Q(t) with 20 % glycol in the fluid

Figure 6.10: Experimental results for increased glycol concentration

The analytical solution holds well against the experimental results, as can be seen in Figure 6.10 and Table 6.9. This is proof that the analytical solution is valid for various viscosities given that the fluid density is known

Concentration [%]	Average discrepancy [%]	Maximum discrepancy [%]
0	1.73	11.31
5	4.76	16.27
15	2.27	12.43
20	3.86	11.61

Table 6.9: Discrepancies with respect to pressure for the varying glycol concentrations

6.6 Effect of fully discharging the accumulator

Something all the prior results have in common is a sudden acceleration in pressure reduction compared to the analytical solution as the accumulator is nearing its pre-charge pressure. The results previously presented in Figure 6.6e can be seen in Figure 6.11 and clearly shows this phenomenon when the accumulator pressure reaches 2.37 bars, or in other words, 6.1 % of the total pressure interval (8.06-2 bars). The pressure reductions for the rest of the experiments are listed in the following tables.

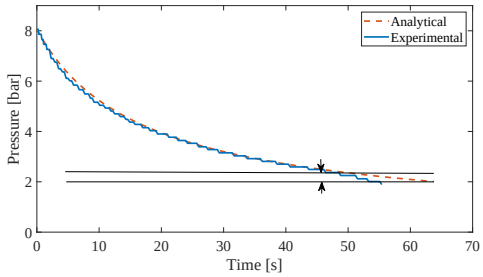

Figure 6.11: Interval of accelerated pressure reduction

Table 6.10 shows how the reduction in discharge time by means of changing the valve orifice also changes the increased pressure reduction when nearing the pre-charge pressure. Valve orifices of 15.40 and 38.10 mm^2 creates such a rapid discharge that irregularities in the pressure drop was not possible to identify.

Valve orifice [mm^2]	Pressure interval [%]	Pressure interval [bar]
2.53	6.60	0.45
6.80	4.52	0.30
11.90	1.10	0.07
15.40	N/A	N/A
38.10	N/A	N/A

Table 6.10: Pressure interval for various valve openings

Table 6.11 displays how the alteration in the internal energy of the gas influences the final acceleration in pressure reduction. The lower the temperature drops, the lower the initial pressure in the accumulator becomes, which in turn gives a smaller total pressure interval. This is the reason why the percentages described in Table 6.11 decrease parallel to the temperature, when in reality the pressure intervals measured in bar are quite similar

for all the temperature tests. This implies a connection between the pre-charge pressure and the point of accelerated pressure reduction

Temperature [°C]	Pressure interval [%]	Pressure interval [bar]
43.00	6.7	0.49
20.00	6.6	0.45
10.38	6.1	0.50
9.35	6.1	0.37
5.71	5.8	0.36
-4.93	4.6	0.49

Table 6.11: Pressure interval for various temperatures

Table 6.12 describes how increased discharge time due to increased viscosity also prolongs the pressure interval of increased pressure reduction. Comparing these results with what is presented in Table 6.11 it can be concluded that altering the internal energy of the gas in the accumulator has a smaller influence on the final pressure interval than what fluid viscosity has. The reduced temperature in the fluid increases its viscosity, but ultimately does not have the same influence as the reduced gas pressure has.

Furthermore, the moment when the accelerated pressure reduction starts for the experiment with a glycol concentration of 20 % occurs at 53.3 seconds. The base case test experiences the same phenomenon at 52.4 seconds, meaning that a 100 % increase in concentration resulted in less than a second of increased, usable discharge time. The test where the accumulator was heated gave a resulting usable discharge time of 54.2 seconds. All three tests have an accelerated pressure reduction interval ranging from 0.45 to 0.5 bars, showing small discrepancies when comparing the three. The only thing in common for the three tests is the accumulator pre-charge, which again indicates a connection between an accumulator's given pre-charge and the point of accelerated pressure reduction.

Glycol concentration [%]	Pressure interval [%]	Pressure interval [bar]
0	5.9	0.39
5	6.0	0.40
10	6.6	0.45
15	7.1	0.48
20	7.7	0.50

Table 6.12: Pressure interval for various glycol concentration

When altering the pre-charge settings of the accumulator Table 6.13 shows significant increases measured in percentage in the interval as the pre-charge increases. The interval measured in bar, however, has rather small variations. All three tests have a pressure interval in the range of 0.45 to 0.51 bars. This also applies for the 2 bar pre-charge tests. Which indicates that the change in pre-charge does not greatly influence the pressure interval when measured in bars.

Pre-charge pressure [bar]	Pressure interval [%]	Pressure interval [bar]
3	10.1	0.67
4	12.8	1.08
5	18.2	1.57

Table 6.13: Pressure interval for various pre-charges

6.7 Umbilical test

For the first umbilical test the accumulator was kept at floor level to establish the effect of tube friction without the impact of gravitational force. The results from test 1 in Figure 6.12 clearly show the effect of friction in the tube as the discharge commences. The analytical solution has not been modified to take gravity and tube friction into consideration as their effects become more visible when presented as it is.

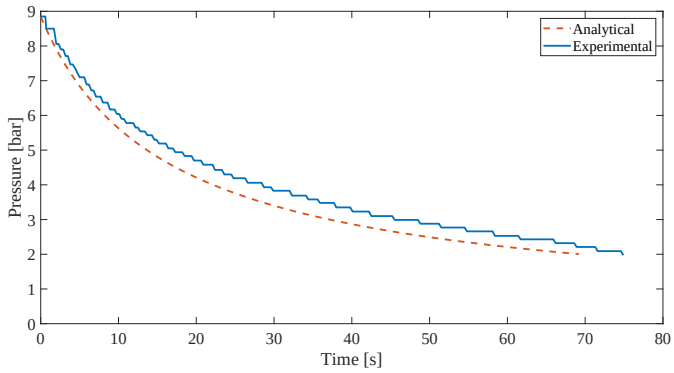

Figure 6.12: Umbilical test 1

For test 2, the accumulator is placed at an elevation of 13.3 meters and the pipe stretches 26 meters along the ground. The discrepancy between the analytical and experimental results regarding P(t) in test 2 compared to those of test 1 are considerably less. This can be explained by the increase in elevation of the accumulator, which increases the fluid velocity in the tube simply due to gravity. As the flow rate decreases towards the end, the analytical and experimental results even out. This can be explained by the previous section, where increased pressure reduction is identified as the accumulator is nearing its pre-charge pressure. The pressure at the end of the tube where the pumps are positioned is plotted in the same figure, denoted *Pressure pump*, where the average pressure difference between the accumulator and the pumps can be seen in Table 6.15.

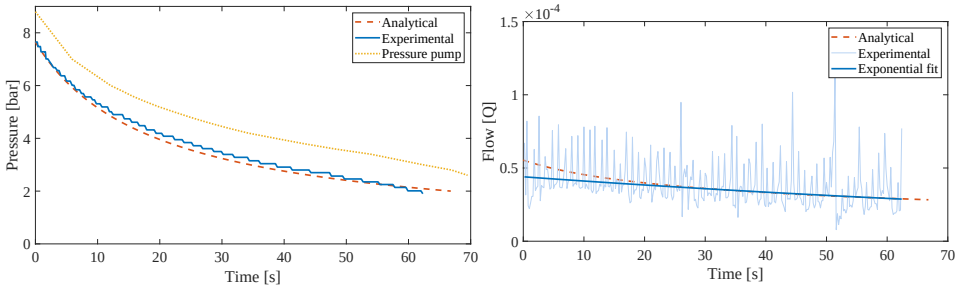

(a) P(t) for umbilical test, 13.3 meter elevation and 26 meters of distance traveled

(b) Q(t) for umbilical test, 13.3 meters elevation and 26 meters of distance traveled

Figure 6.13: Umbilical test 2

Test 3, visible in Figure 6.14, show the first of 3 tests where the tube length has been doubled compared to that of test 1 and 2, then gradually shortened. When comparing test 3 and 4, there is a clear difference with respect to the time it takes to fully discharge the accumulator. The difference in charge pressure due to the increase in elevation from test 3 to 4 has a considerable impact on the discharge time as test 4 has a 5.1 second shorter discharge. The distance the tube travels at the bottom of the stairwell is in this case decreased due to the increased elevation. When comparing test 4 and 5, the only change made to the system is the length of the tube, which only impacts the length travelled after reaching the bottom of the stairwell. It is clear to see in test 5 that the 12-meter reduction in tube length has decreased the friction in the tube, and as a result also decreased the discharge time. Figure 6.16a shows a high level of correlation between the experimental result and analytical solution when the ratio between tube height and distance travelled along the ground is 1:1.9.

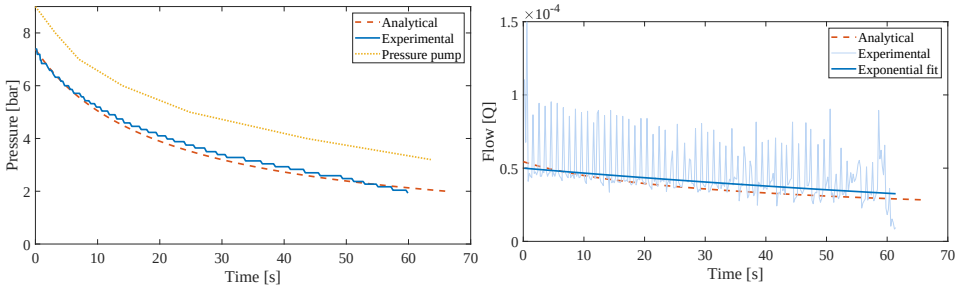

(a) P(t) for umbilical test, 17.6 meter elevation and 58 meters of distance travelled

(b) Q(t) for umbilical test, 17.6 meter elevation and 58 meters of distance travelled

Figure 6.14: Umbilical test 3

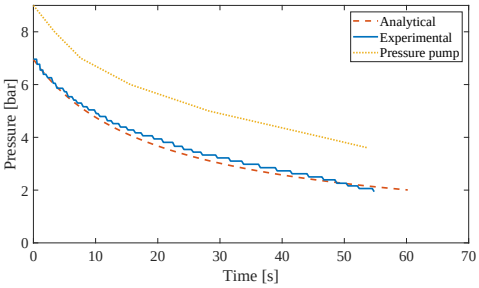

(a) P(t) for umbilical test, 21.9 meter elevation and 54 meters of distance travelled

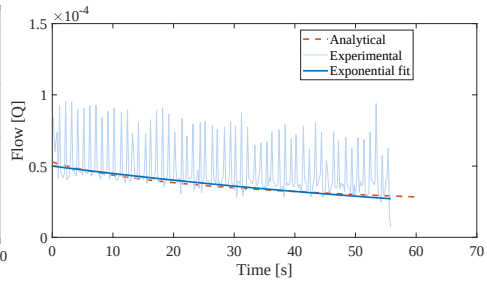

(b) Q(t) for umbilical test, 21.9 meter elevation and 54 meters of distance travelled

Figure 6.15: Umbilical test 4

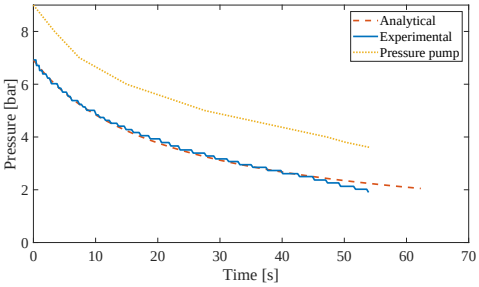

(a) P(t) for umbilical test, 21.9 meter elevation and 42 meters of distance travelled

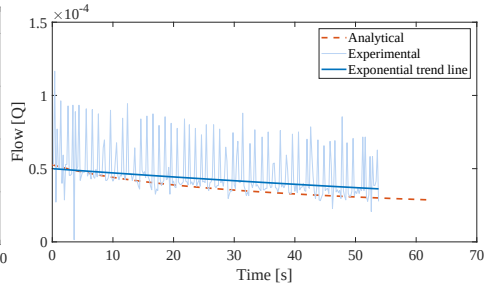

(b) Q(t) for umbilical test, 21.9 meter elevation and 42 meters of distance travelled

Figure 6.16: Umbilical test 5

Test number	Average discrepancy [%]	Maximum discrepancy [%]
1	10.32	15.14
2	4.18	10.21
3	4.19	10.47
4	4.46	8.56
5	2.56	18.05

Table 6.14: Discrepancies between the experimental results and the analytical solution for umbilical tests

Test number	$P_{loss_{avg}}$ [bar]
2	1.04
3	1.38
4	1.74
5	1.77

Table 6.15: Average pressure difference between the accumulator and the point of discharge for the umbilical tests

6.8 Isothermal process

For the isothermal test result, there is no analytical solution to compare with. The opening of the valve, as mentioned earlier, has such a small orifice that the discharge can be characterized as leakage. This makes it impossible to determine the area of the valve opening, and as a result there can be no analytical solution. However, the test has given quite interesting results. Figure 6.17a carries a close resemblance to what is witnessed after 40 seconds in the field data supplied by OneSubsea in Figure 6.18. The theory for what is happening before this is that a water hammer occurs (Vidal, 2018), due to the rapid separation of the pump and the umbilical line, resulting in a considerable pressure reduction in the system.

To achieve the most accurate results with respect to recreating OneSubea's system, the valve which the accumulator discharges through was never blocked but was allowed to have fluid flow through it while the pumps pressurized the accumulator. The reason for this was that the accumulator would start its discharge the moment valve V-03 (Figure 3.1) was closed. This is in line with what happens in the actual system, where the accumulator is not allowed to go through an isochoric process before discharging.

The thermal time constant in the gas has been calculated to be 50 seconds. The first 100 seconds of operation in both Figure 6.17a and 6.17b show a rapid reduction in both pressure and flow rate. This corresponds to a certain degree with the thermal time constant and is an indicator of what is happening in the accumulator regarding the rapid pressure reduction that OneSubsea is experiencing. It should also be mentioned that all other experiments done in the previous sections also experience higher initial pressure loss, simply due to greater pressures at the start of the discharge period and should therefore also be considered when analysing the results. On the other hand, upon discharge the gas is experiencing reduced internal energy not only due to fluid leaving the accumulator which lets the gas expand. The increased temperature in the gas due to the initial compression also results in the gas exchanging heat with its surroundings, meaning that the rapid pressure reduction will continue until the gas temperature is the same as that of its surroundings.

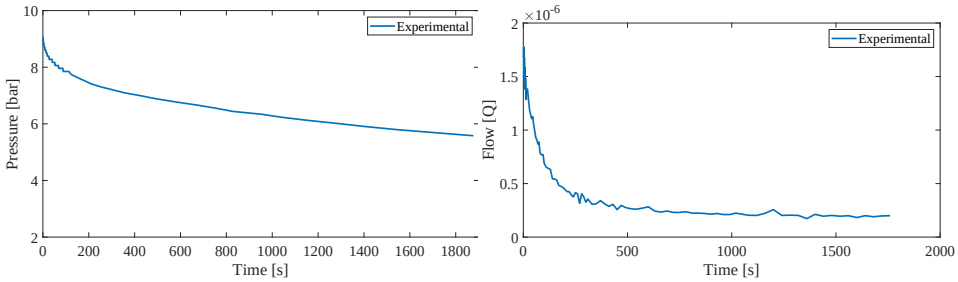

(a) P(t) for isothermal test

(b) Q(t) for isothermal test

Figure 6.17: Test results for isothermal experiment

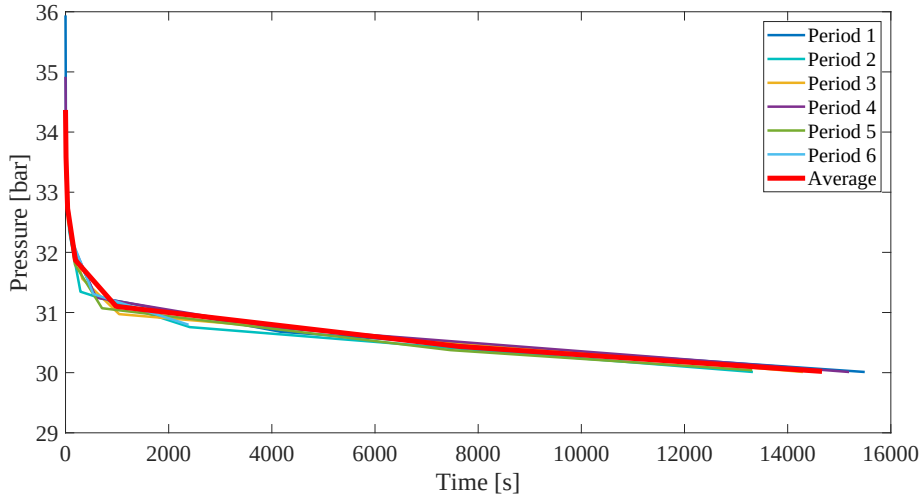

Figure 6.18: Graph of the accumulators field data provided by OneSubsea on an off-shore installation.

6.9 Dimensionless presentation of results

To obtain more generalized results that can be compared to other experiments or CFD-models, all the experimental results have been plotted in a logarithmic scale where all parameters have been made dimensionless. To create dimensionless parameters for pressure and time, the equations below are used for the x and y-axis respectively

$$x = ln\frac{t}{\omega} \tag{6.2}$$

$$y = ln\frac{p}{p_0} \tag{6.3}$$

where p is the pressure in the accumulator at a given time, p_0 is the initial pressure in the accumulator at full charge, t is the time and $\omega = \frac{V}{Q}$, where V is the total volume of the accumulator and Q is the maximum theoretical flow through the valve orifice calculated with Equation 4.3. The results for the various valve openings, pre-charge pressures, glycol concentration and temperatures are given in the following Figures

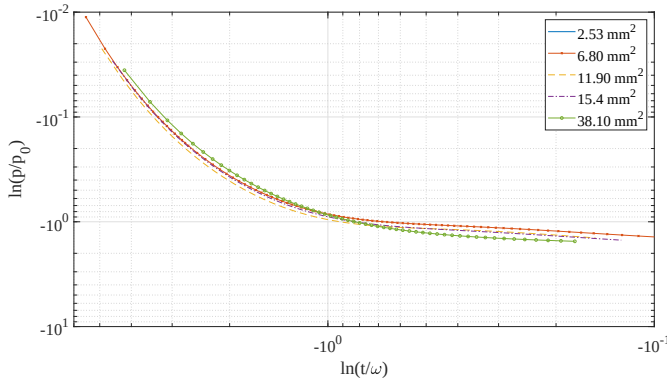

Figure 6.19: Dimensionless plot of the experimental results for altered valve openings

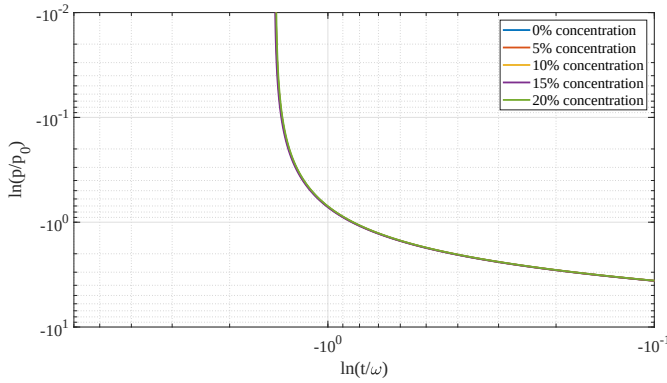

Figure 6.20: Dimensionless plot of the experimental results for altered glycol concentrations

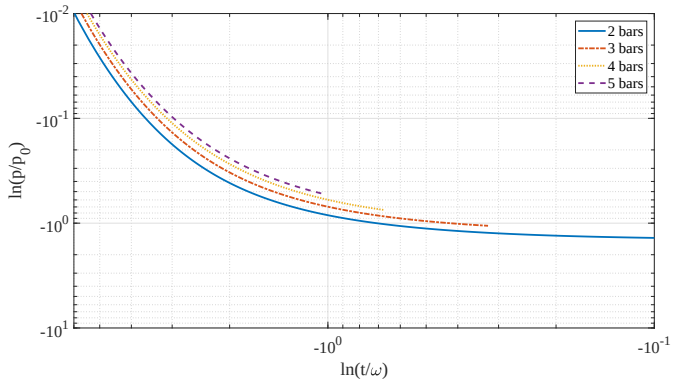

Figure 6.21: Dimensionless plot of the experimental results for altered pre-charge pressures

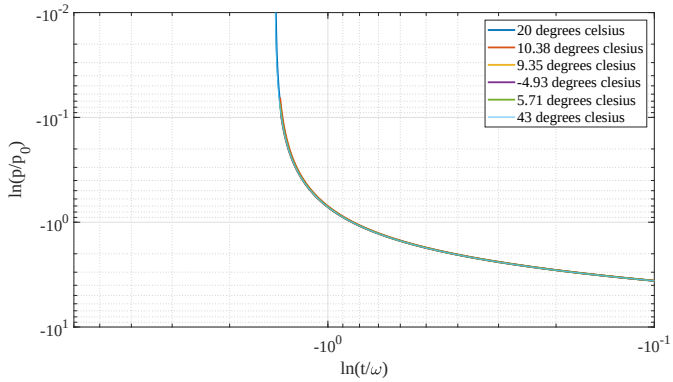

Figure 6.22: Dimensionless plot of the experimental results for altered glycol concentrations

The linear regression for all of the results have been plotted, as can be seen in Appendix B. The tangent to the angle, ϕ, between the linear regression and the x-axis and the Reynolds number, calculated with Equation 2.43 based on the maximum theoretical fluid velocity, has been found for all the experimental results and is listed in Appendix B.1. A scatter plot for these results is presented in Figure 6.23

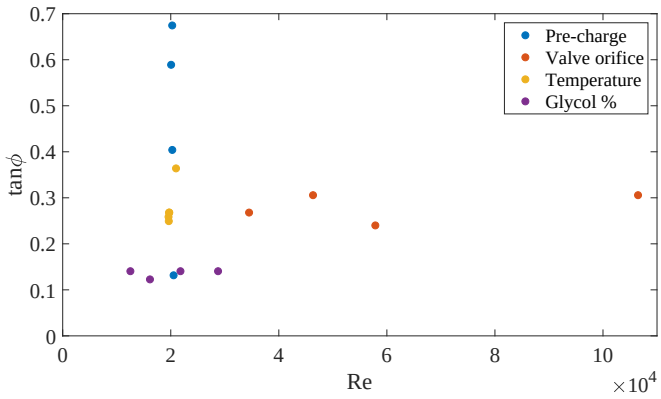

Figure 6.23: Scatter plot for all experimental results

As previously explained, the dimensionless plots are to be used to evaluate CFD-models (Hiis, 2018) up against the experimental results obtained. Data obtained from Hiis (2018) where a bladder accumulator with a set of three individual discharge orifices is listed in Table 6.16 together with the corresponding experimental data.

Discharge orifice	ϕ	**tanϕ**	**Re**	
2.53 mm^2	10.5	0.1853	20526	CFD
15.4 mm^2	11	0.1944	57864	CFD
38.1 mm^2	15	0.2679	106487	CFD
2.53 mm^2	7.5	0.1316	20526	Experimental
15.4 mm^2	13.5	0.2400	57864	Experimental
38.1 mm^2	17	0.3057	106487	Experimental

Table 6.16: Data from CFD-model and experiments

The data listed above has been plotted in Figure 6.24 and shows correlating results for the experimental results and the CFD-model.

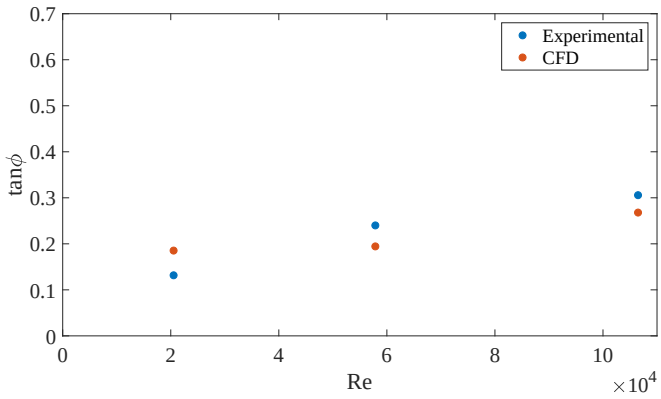

Figure 6.24: Data comparison of specific CFD-models and experiments

A scatter plot where all dimensionless experimental results from this thesis and CFD-models presented by Hiis (2018) is shown in the table below. The data can be seen in Appendix B.1 and B.2.

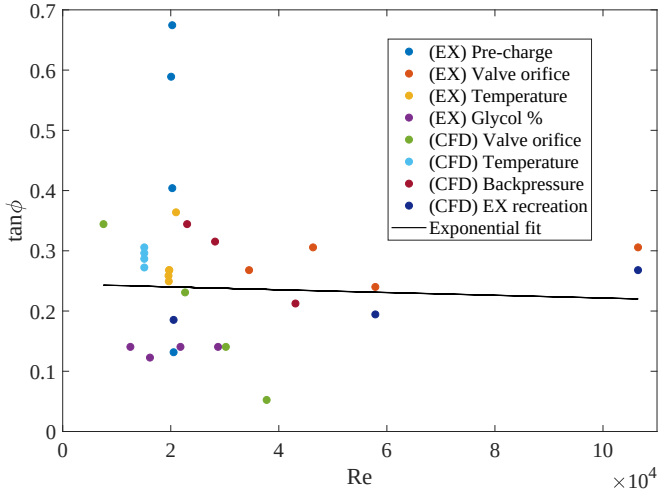

Figure 6.25: Data comparison of all CFD-models and experiments

Chapter 7

Conclusion

Two main categories of experiments have been conducted on a 4 l hydraulic bladder accumulator for this thesis: umbilical and non-umbilical tests. The non-umbilical tests uncovered in detail how various conditions impacts the performance of a hydraulic accumulator with respect to discharge.

Cooling or heating of the accumulator does not affect its behaviour while discharging adiabatically beyond the change in the internal energy in the gas, affecting the initial charge pressure in the accumulator. The glycol concentration of the hydraulic fluid used for the experiments has a substantial effect on the accumulator's discharge. The time it takes to discharge the accumulator increases exponentially as the concentration increases. This is connected to the rise in viscosity which also increases exponentially with the glycol concentrations.

The increase in pre-charge pressure, which in turn reduces the compression rate of the accumulator, influences the discharge time in the sense that the accumulator has less fluid to discharge.

Tests where an umbilical system has been replicated has shown the effect of tube friction and gravity acting on the hydraulic fluid. Where a tube height to length ratio of 1:1.9 gave highly correlating results with respect to the experimental results and the analytical solution.

The analytical solution has been thoroughly tested and validated against all experiments described in the thesis and holds well for all tests. For all non-umbilical tests, the average discrepancies between the analytical solution and experimental results is 4.73 % or lower, while for the umbilical tests where the accumulator was at an elevation the average discrepancies were all less than 4.46 %, clearly indicating high levels of precision in the analytical solution.

Isothermal experiments resulted in findings quite similar to those of OneSubsea. When the accumulator is allowed to discharge continuously also while being recharged by a pump, an isochoric process is never initiated in the gas. When the gas is compressed, its temperature together with its internal energy increases. The heat in the gas will transfer to its surroundings until it reaches its surrounding temperature, resulting in a more rapid pressure reduction in the accumulator for the first part of the discharge cycle.

Recommendations for future work

As all experiments in this thesis are carried out with a bladder accumulator and OneSubsea's system consists of piston accumulators, it would be of interest to investigate the behaviour of a piston accumulator going through similar tests. The use of a piston accumulator would also enable monitoring of the gas-chamber with respect to both pressure and temperature. It would be highly beneficial to be able to monitor the temperature change in the gas by means of a low thermal response time temperature element to further investigate the results presented in this thesis.

With respect to the umbilical tests, alterations such as placing the pumps at the same elevation as the accumulator and using a long tube strong enough to hold pressures of 8 to 9 bars over an extended period would be beneficial. This would increase the total pressure in the accumulator and enable isothermal umbilical tests, which would be a more correct recreation of OneSubsea's system.

Bibliography

Cimberion, 2018. Cimberio valve cim50.
URL http://nrfportal.vvsnrf.no/produkt-detaljer?pn=5512374

Haugland, B. R. S., Wikan, D. B., 2017. Fluidsim model development at onesubsea.

Hiis, E., 2018. Computational study of hydraulic accumulators.

Hiis, E., Stenhjem, M. A., 2017. Analysis of accumulator discharge.

Hoffmann, A. C., September 2017a. Fluid dynamics, the overall picture.

Hoffmann, A. C., October 2017b. Heat transfer and its applications.

Hoffmann, A. C., October 2017c. Radiation.

Juhala, J., Kajaste, J., Pietola, M., 2014. Experimental analysis of heat losses in different types of hydraulic accumulators. In: 8th FPNI Ph. D Symposium on Fluid Power. American Society of Mechanical Engineers, pp. V001T03A003–V001T03A003.

Kjølle, A., 1989. Oljehydraulikk. Tapir Forlag.

Lewis, R. W., Nithiarasu, P., Seetharamu, K. N., 2004. Fundamentals of the finite element method for heat and fluid flow. John Wiley & Sons.

Otis, D., Pourmovahed, A., 1985. An algorithm for computing nonflow gas processes in gas springs and hydropneumatic accumulators. Journal of dynamic systems, measurement, and control 107 (1), 93–96.

Pourmovahed, A., Otis, D., 1990. An experimental thermal time-constant correlation for hydraulic accumulators. Journal of dynamic systems, measurement, and control 112 (1), 116–121.

RS, 1999. Jumo PT100 Sensor -50C min +270C max 29mm length x 7.5mm diameter kernel description.
URL https://uk.rs-online.com/web/p/platinum-resistance-temperature-sen
1584385/

Rydberg, K.-E., 2013. Hydraulic fluid properties and their impact on energy efficiency. In: 13th Scandinavian International Conference on Fluid Power, June 3-5, 2013, Linköping, Sweden. Linköping University Electronic Press, pp. 447–453.

Rydberg, K.-E., 2015. Energy efficient hydraulics: System solutions for loss minimization. In: The National Conference on Fluid Power," Hydraulikdagar'15" Linköping, Sweden, March 16-17, 2015.

Singireddy, S. R., Javalagi, S., 2012. Hydraulic fluid properties and its influence on system performance.

Teja, A. S., 1983. Simple method for the calculation of heat capacities of liquid mixtures. Journal of chemical and engineering data 28 (1), 83–85.

TETRA, 2005. Engineered Soultions Guide For Clear Brine Fluids And Filtration.

Toolbox, E., 2003a. Air - thermophysical properties.

Toolbox, E., 2003b. Overall heat transfer coefficients for fluids - heat exchanger surface combinations.

Vidal, J. G., 2018. Pragmatic numerical models of a subsea hydraulic accumulator.

Yoshida, F., Iio, S., Ito, K., Kitagawa, A., 2017. Experimental and theoretical analysis of active charge accumulator for water hydraulics system. IEEE Access 5, 881–890.

Appendix

Appendix A

Aditional experiments

A.1 Altered pre-charge

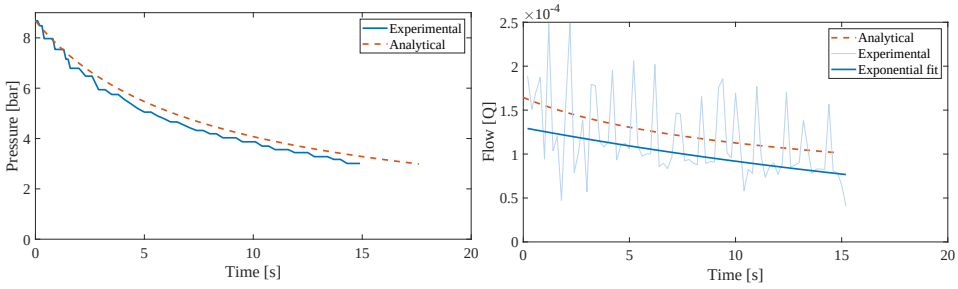

(a) P(t) with 6.80mm^2 valve opening and 3 bars of precharge

(b) Q(t) with 6.80mm^2 valve opening and 3 bars of precharge

Figure A.1: Experimental results for 3 bars of pre-charge and 6.80 mm^2 valve orifice

A.2 Altered temperatures

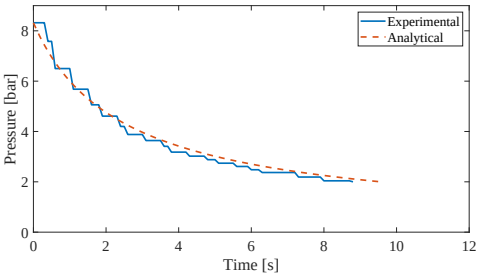

(a) P(t) with 15.4mm^2 valve opening and setting 1 in refrigerator

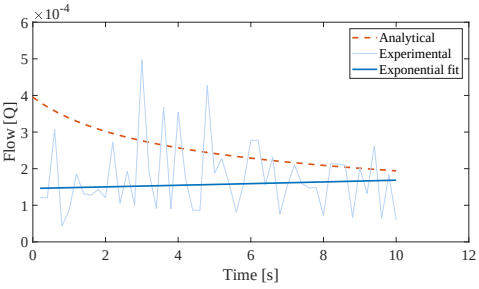

(b) Q(t) with 15.4mm^2 valve opening and setting 1 in refrigerator

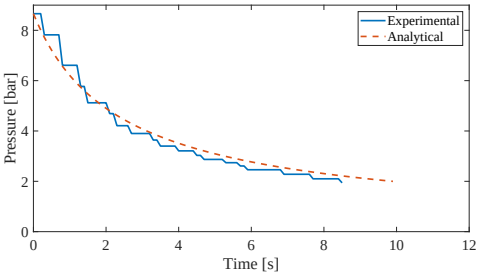

(c) P(t) with 15.4mm^2 valve opening and setting 4 in refrigerator

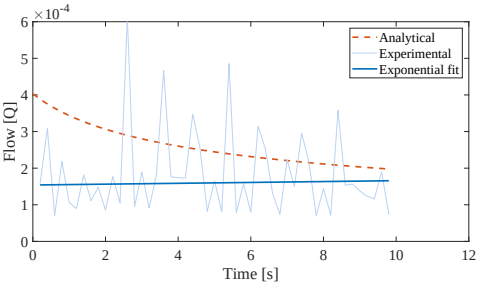

(d) Q(t) with 15.4mm^2 valve opening and setting 4 in refrigerator

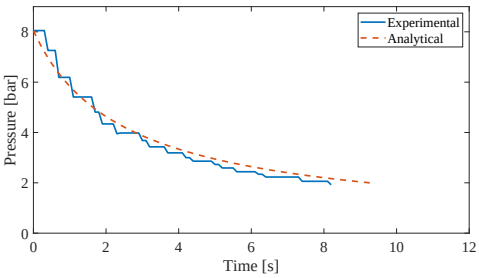

(e) P(t) with 15.4mm^2 valve opening and setting 7 in refrigerator

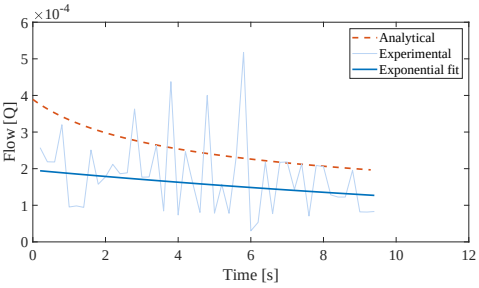

(f) Q(t) with 15.4mm^2 valve opening and setting 7 in refrigerator

Figure A.2: Altering temperatures for 15.4mm^2 valve opening

Appendix B

Dimensionless analysis data

Pre-charge [bar]	**A$_{valve}$ [mm^2]**	**T$_{acc}$ [°C]**	**Glycol [%]**	ϕ	**tanϕ**	**Re**
2	2.53	20	10	6.5	0.1139	20526
3				22	0.4040	20281
4				30.5	0.5890	20268
5				34	0.6745	20269
2	6.80	20	10	15	0.2679	34495
	11.90			17	0.3057	46332
	15.44			13.5	0.2400	57864
	38.10			17	0.3057	106487
2	2.53	43	10	20	0.3639	20973
		10.38		15	0.2679	19697
		9.35		14.5	0.2586	19588
		-4.93		14	0.2493	19637
		-4.93		15	0.2679	19721
2	2.53	20	0	8	0.1405	28754
			5	8	0.1405	21796
			15	7	0.1227	16151
			20	8	0.1405	12527

Table B.1: All angles and Reynolds numbers for the experiments

$\mathbf{A}_{valve}$ [mm^2]	Back pressure [bar]	$\mathbf{T}_{acc}$ [°C]	ϕ	tan(ϕ)	Re
78.54	30.7	20	3	0.0524	37750
50.26	30.7	20	8	0.1405	30200
28.27	30.7	20	13	0.2309	22650
12.56	30.7	4	17	0.3057	15100
12.56	30.7	12	16.5	0.2962	15100
12.56	30.7	20	16	0.2867	15100
12.56	30.7	27	15.5	0.2773	15100
12.56	25	20	19	0.3443	23027
12.56	20	20	17.5	0.3153	28202
12.56	0	20	12	0.2125	43080
3.14	30.7	20	19	0.3443	7550

Table B.2: All angles and Reynolds numbers from CFD-models (Hiis, 2018)

B.1 Altering temperature

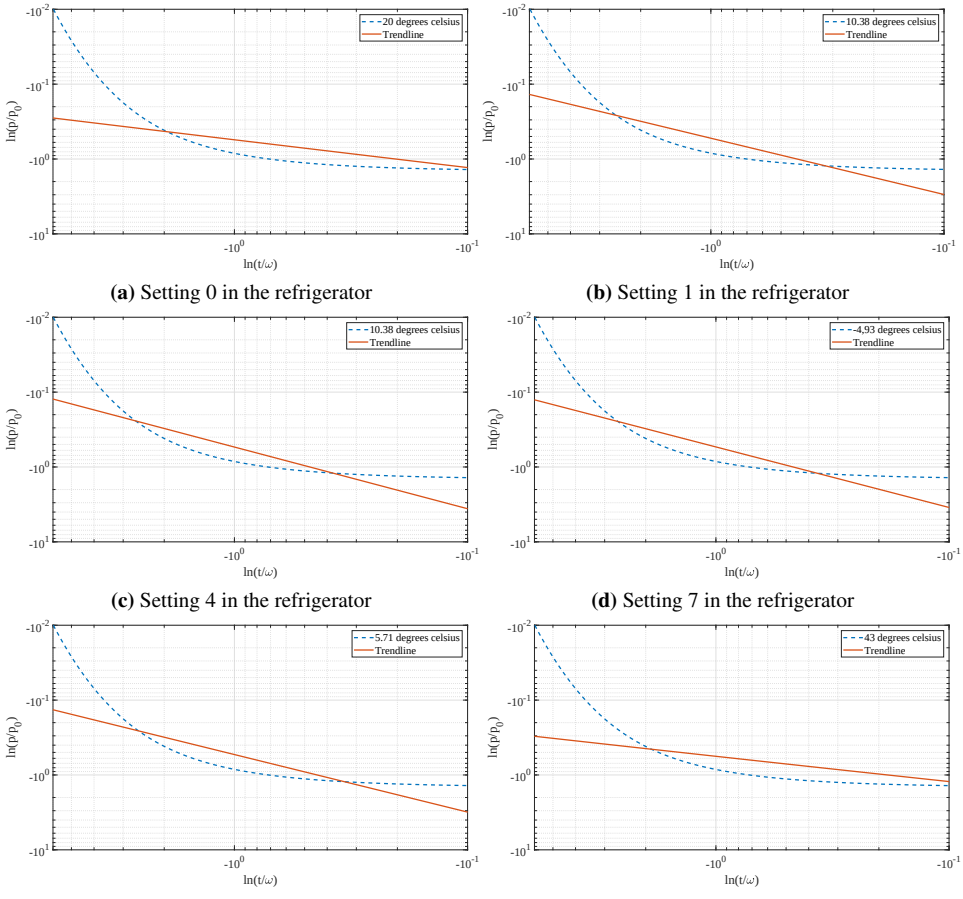

(a) Setting 0 in the refrigerator

(b) Setting 1 in the refrigerator

(c) Setting 4 in the refrigerator

(d) Setting 7 in the refrigerator

(e) Natural convection (cooling)

(f) Natural convection (heating)

Figure B.1: Dimensionless plots with various temperatures with a valve opening of 2.53 mm^2

B.2 Altering valve opening area

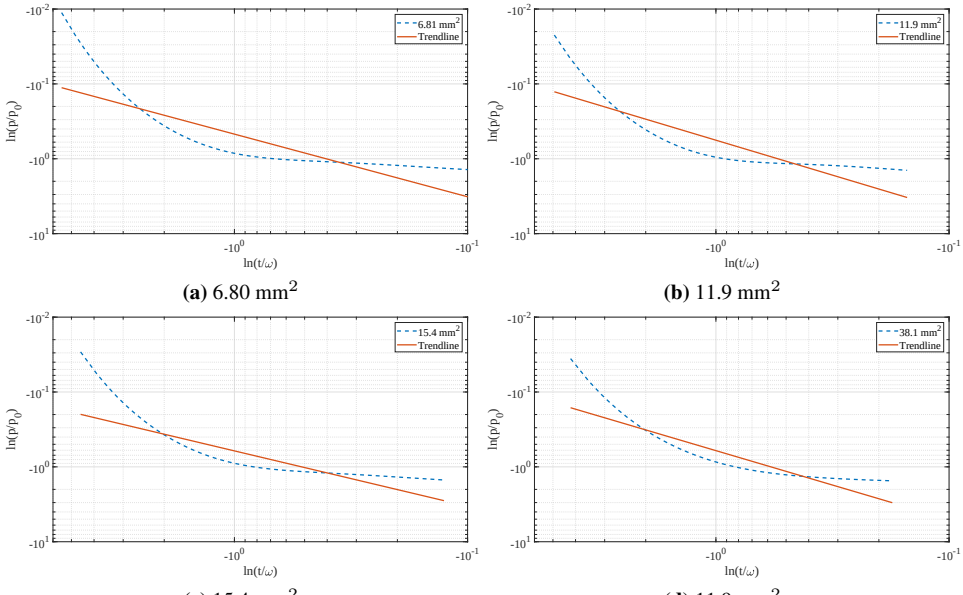

(a) 6.80 mm^2 **(b)** 11.9 mm^2

(c) 15.4 mm^2 **(d)** 11.9 mm^2

Figure B.2: Dimensionless plots for various valve openings

B.3 Altering pre-charge pressure

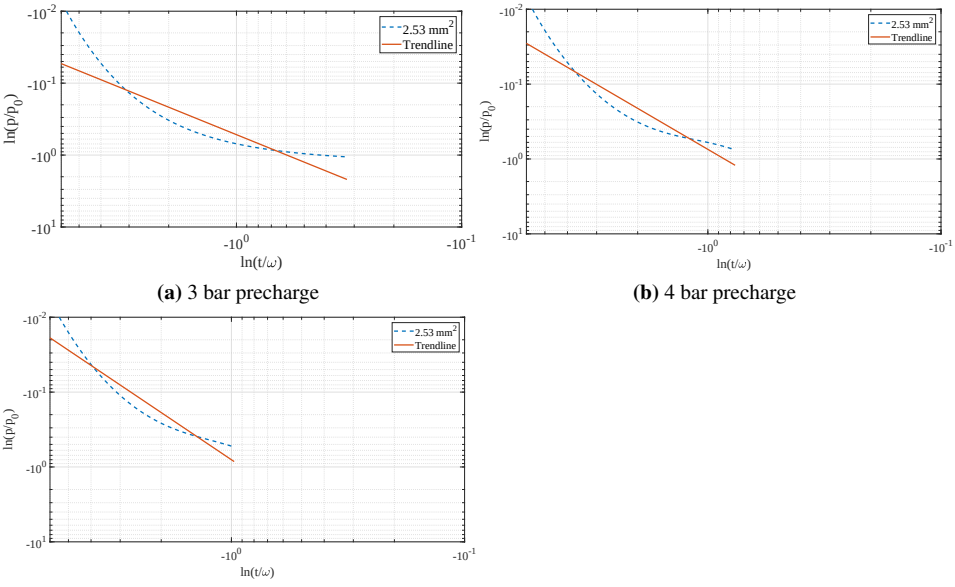

(a) 3 bar precharge

(b) 4 bar precharge

(c) 5 bar precharge

Figure B.3: Dimensionless plots for 3, 4 and 5 bar pre-charge with a valve opening of 2.53 mm^2

B.4 Altering glycol concentration

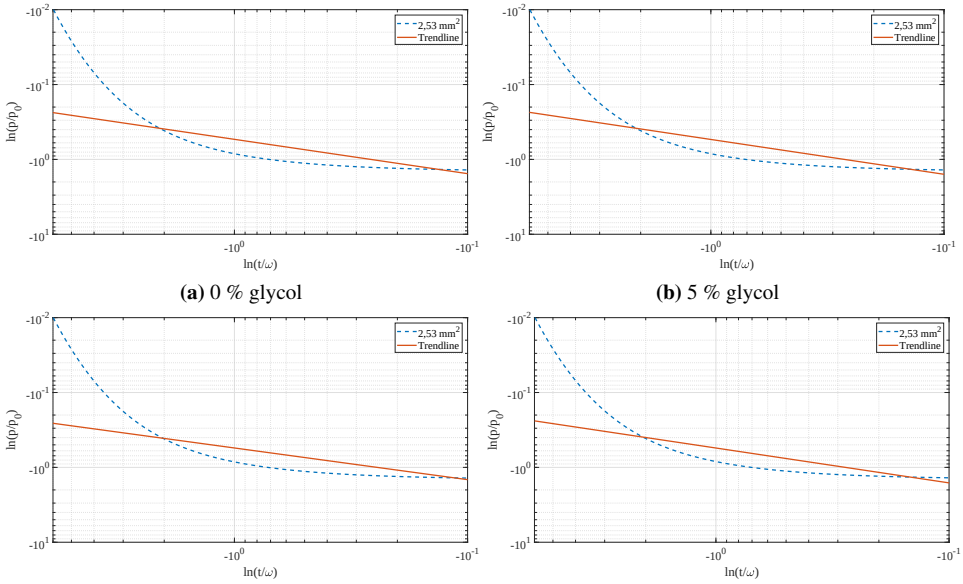

(a) 0 % glycol

(b) 5 % glycol

(c) 15 % glycol

(d) 20 % glycol

Figure B.4: Dimensionless plots for various glycol concentrations with a valve opening of 2.53 mm^2